Cryptotephra in the East Antarctic Mount Brown South ice core

Margaret Harlan[1,2,3,4], Jodi Fox[3,5], Helle Astrid Kjær[2], Tessa Vance[1], Anders Svensson[2], and Eliza Cook[2]

[1]Australian Antarctic Program Partnership, Institute for Marine and Antarctic Studies, University of Tasmania, Hobart, Australia
[2]Physics of Ice, Climate, and Earth, Niels Bohr Insitute, University of Copenhagen, Denmark
[3]Institute for Marine and Antarctic Studies, University of Tasmania, Hobart, Australia
[4]Canadian Ice Core Lab, Earth and Atmospheric Sciences, University of Alberta, Edmonton, Canada
[5]Department of Geology and Paleontology, National Museum of Nature and Science, Tsukuba, Japan

Correspondence: Margaret Harlan (mharlan@ualberta.ca)

Abstract. Ice cores contain stratified layers of impurities scavenged from the atmosphere, which are a vital tool for investigating the Earth system. Reconstructing past eruption records by way of ice core tephrochronology can help us understand ash dispersal, atmospheric circulation processes, and the impacts of volcanic eruptions on climate. This study presents the coastal East Antarctic Mount Brown South (MBS, 69.11°S, 86.31°E; 2084 m ASL) ice core as an untapped tephrochronological archive. We utilize a customized cryptotephra sampling plan, integrating ice core data, HYSPLIT air parcel trajectories, and known eruption records, and identify two distinct cryptotephra horizons at ∼13.3 and ∼17.9 m depth in the MBS-Alpha ice core. We also find sparse cryptotephra grains from various unidentified sources throughout the core. Through geochemical characterization with electron probe microanalysis (EPMA), we correlate the two cryptotephra horizons with the 1991 eruption of Cerro Hudson and the continuous eruptions of Mt. Erebus throughout the mid-1980s. The volcanic horizons identified here underscore the role of MBS in extending the regional volcanic record, helping to constrain ice core dating efforts, and enhancing understanding of volcanic ash dispersal to East Antarctica.

1 Introduction

Ice core records are important archives of the changing Earth system. They record recent climate events in detail, including volcanic eruption histories, and in some cases the strength and source of such eruptions (Svensson et al., 2020; Sigl et al., 2014; Lowe, 2011; Abbott et al., 2024; Narcisi et al., 2012; Kurbatov et al., 2006; Dunbar et al., 2003). Ice sheets and ice caps can contain both soluble (e.g. volcanic sulfate) and insoluble volcanic products (e.g. ash), deposited on the ice, providing valuable information on past volcanic eruption histories. Analyzing these products in ice cores can deepen our understanding of volcanic climate forcing, and help to refine ice core chronologies (Gao et al., 2008; Castellano et al., 2004; Sigl et al., 2014, 2015; Lohmann and Svensson, 2022; Lin et al., 2022).

Tephrochronology, the use of tephra (used here to refer to any material ejected during explosive volcanic eruptions, and in ice core studies, typically ash sized ($\leq$ 2 mm; McPhie et al. (1993))) and cryptotephra (any tephra not visible to the naked eye, due to either sparseness or small grain size) as isochronous horizons in stratigraphic archives such as ice cores and sediment records can be used to date archives, synchronize geographically distinct records, and inform about past volcanic events (Lowe,

2011; Geyer et al., 2023; Cook et al., 2022). While volcanic horizons can be identified by soluble tracers including volcanic sulfate, acidity, and non-sea-salt conductivity, characterization and geochemical fingerprinting of tephra and cryptotephra can be used to identify the specific volcanic sources for eruption events (Lowe, 2011; Cook et al., 2018; Winstrup et al., 2019; Svensson et al., 2020; Lin et al., 2022; Geyer et al., 2023).

Ice core records are often geographically distal or ultra-distal (up to thousands of kilometers away or more) archives of volcanic ash, and the tephra found are typically micrometer-scale volcanic glass shards from volcanic ash fallout transported long distances by atmospheric circulation processes (Lowe, 2011; Geyer et al., 2023). Locating and identifying cryptotephra in ice cores is especially difficult, as volcanic markers such as sulfate, conductivity, or acidity do not always co-occur with tephra deposits from the same eruption, and comprehensive sampling must be undertaken to produce a full tephrochronological framework (Cook et al., 2018; Lin et al., 2022; Abbott et al., 2024; Lowe, 2011; Narcisi et al., 2010; Cook et al., 2022; Basile et al., 2001).

Tephra previously identified in other studies of Antarctic ice cores and blue ice areas come from local and regional sources, including Antarctic (Narcisi et al., 2006; Basile et al., 2001; Abbott and Davies, 2012; Iverson et al., 2017) and sub-Antarctic island volcanoes (Basile et al., 2001; Abbott et al., 2024; Narcisi et al., 2012). Additionally, tephra found in Antarctic ice and snow has been correlated to large eruptions from ultra-distal sources e.g. Aotearoa New Zealand (Taupō; Dunbar et al. (2017)), South America (Cerro Hudson, Puyehue-Cordón Caulle; Abbott et al. (2024); Narcisi et al. (2012); Koffman et al. (2017)), and possibly even Mexico (El Chichón; Palais et al. (1992)).

Many efforts in recent years have been undertaken to improve Antarctic tephrochronologies, using ice cores from across the continent including Talos Dome (Narcisi et al., 2012), Siple Dome (Kurbatov et al., 2006), Vostok (Basile et al., 2001; Narcisi et al., 2010), and others (Abbott et al., 2024; Narcisi et al., 2005, 2010). Ice cores spanning millenia can be used to produce tephrochronologies covering the Holocene or Last Glacial period, often with an aim to constrain timings of changes to global climate (Lin et al., 2022; Lohmann and Svensson, 2022; Cook et al., 2022; Castellano et al., 2004; Abbott and Davies, 2012). Ice cores from higher accumulation sites such as WAIS-Divide and Law Dome, on the other hand, can provide important means for investigating volcanic eruptions and climate in detail in the more recent past (Abbott et al., 2024; Plunkett et al., 2023; Piva et al., 2023; Narcisi and Petit, 2021; Sigl et al., 2014, 2013; Narcisi et al., 2012; Gao et al., 2008).

Volcanic products most commonly identified in Antarctic ice core records include those from Antarctic (e.g. Mt. Erebus) and Sub-Antarctic island volcanoes (including South Sandwich and South Shetland Islands), as well as lower latitude volcanoes in Chile and Aotearoa New Zealand (Narcisi et al., 2012; Dunbar et al., 2017; Koffman et al., 2017). A number of volcanoes with the potential to disperse volcanic material to Antarctica have been active during the satellite era (1979 to present) (Global Volcanism Program, 2024). Such satellite era eruption events are typically well observed through comprehensive monitoring programs and satellite remote sensing (Global Volcanism Program, 2024; Francis et al., 1996; Poland et al., 2020).

The Mount Brown South (MBS) ice cores, comprising an intermediate ice core ($\sim$290.5 m in length) and three surface cores ($\sim$20 - 26 m in length), were drilled in coastal East Antarctica during the 2017-2018 austral summer field season (69.11°S, 86.31°E, 2084 m ASL; Fig. 1). The MBS cores provide a new, high resolution climate archive spanning 1137 years, with shallow cores providing duplicate records from 1979 to 2017 (Vance et al., 2024a).

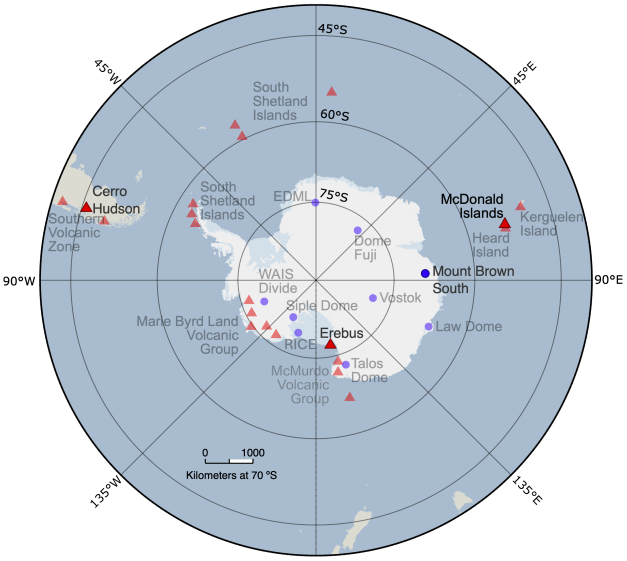

Figure 1. Map of Antarctica showing the location of the ice core sites (blue circles) and volcanic regions of interest (red triangles) relevant to this study. Locations directly related to this study (Mount Brown South, McDonald Islands, Erebus, and Cerro Hudson) are shown in bold colors/text. (Basemap provided by the SCAR Antarctic Digital Database, accessed via the Norwegian Polar Institute's Quantarctica package (Matsuoka et al., 2018)).

The MBS site was selected for its teleconnections and strong climatological link to the Southern Indian Ocean, providing a millenial-length past climate record for a region underrepresented in the existing array of Antarctic ice core records (Vance et al., 2016, 2024a). Subsequent analyses have shown that East Antarctic ice core records (from MBS as well as the Law Dome ice core) provide insight into past climate conditions. East Antarctic records have preserved anthropogenic changes to atmospheric greenhouse gases (Etheridge et al., 1996), El Niño-Southern Oscillation (Crockart et al., 2021) and Australian hydroclimate and bushfire conditions (Udy et al., 2022, 2024), as well as regional events including atmospheric rivers and extreme precipitation events (Jackson et al., 2023; Gkinis et al., 2024b; Zhang et al., 2023).

Due to its coastal Antarctic location, as well as the known teleconnections across the region (Vance et al., 2016; Crockart et al., 2021), we propose that MBS is well situated among the Antarctic ice core array to receive and store wind-blown volcanic ash, making it a useful tephrochronological archive. We present an investigation of cryptotephra in the MBS ice cores, in order to assess potential preservation of volcanic ash, and better characterize the tephra transport pathways in the region. This study focuses on the satellite era record from MBS (1979 to 2017) as a first investigation of cryptotephra in MBS. Our characterization of the cryptotephra horizons together with atmospheric modeling and satellite derived data will inform future design and interpretation of tephrochronology paleo-record studies of MBS and ice cores across Antarctica.

2 Materials and methods

2.1 Mount Brown South ice cores

The MBS-Main core (4.25-294.785 m depth) is supported by three surface firn cores: MBS-Alpha (surface to 20.41 m depth), -Bravo (surface to 20.225 m depth), and -Charlie (surface to 25.89 m depth). Mean accumulation rates derived by annual layer counting throughout the satellite era are 0.309±0.08 m yr-1 ice equivalent (IE) for the main core and 0.298±0.07 m yr-1 IE for the MBS-Alpha core (Crockart et al., 2021). This correlates with the ERA5 estimated site annual accumulation of 0.302±0.05 m yr^{-1} IE (Crockart et al., 2021). The climatology and site conditions of Mount Brown South are discussed in detail in Vance et al. (2016, 2024a), Crockart et al. (2021) and Jackson et al. (2023).

The MBS-Main and MBS-Alpha cores have been analyzed for both trace impurities and stable water isotopes (δ^{18}O) (Gkinis et al., 2024a, b; Jackson et al., 2023). Measurements were performed on discrete samples at 3 cm resolution, using ion chromatography (chemistry/trace impurities, Vance et al. (2024b); Harlan et al. (2024b)) and cavity ring down spectroscopy (stable water isotopes, Moy et al. (2024); Gkinis et al. (2024b)) at the Institute for Marine and Antarctic Studies at the University of Tasmania and Physics of Ice, Climate and Earth, Niels Bohr Institute, at the University of Copenhagen. Additionally, the MBS-Main core was analyzed using continuous flow analysis (CFA) for trace impurities (Harlan et al., 2024b) and stable water isotopes (Gkinis et al., 2024b), also at the University of Copenhagen.

Limited sample material remains of the MBS-Main core throughout the satellite era depths, after re-sampling was required due to challenges with contamination during discrete chemistry sampling. The outer edge pieces remaining after preparation of samples for CFA remain available to use, but the sample size is small ($\sim$2cm^2). The MBS-Alpha core, had a much larger remaining sample area usable for this study ($>$10 cm^2). Part of the MBS-Alpha core was damaged in a freezer failure, resulting in some sections with one slightly melted edge along the length of the core. The trace chemistry samples from the damaged cores appear to be reliable (see Vance et al. (2016)) and the damaged edges of the core have been removed. While the core is not suitable for analyses where high temperature or slight meltwater migration would compromise the results, the cores are still able to be used for microparticle analysis, including tephra studies.

The chemistry and stable water isotopes for the MBS-Main and MBS-Alpha cores have been analyzed and compared across cores (Crockart et al., 2021). The cores align well, and robust chronologies have been produced for both cores (Crockart et al., 2021; Vance et al., 2024a). The MBS-Main and surface cores have been dated using independent layer counting and volcanic matching. A thorough description of the process of chronology development and the resulting age scale (MBS2023) is presented in Vance et al. (2024a). The MBS2023 chronology provides depths for annual horizons for the main and surface cores (Vance et al., 2024b). Thanks to the robust chronology development efforts for these cores, we are able to cross-match depths across the MBS ice core array, allowing us to make use of the multiple cores to provide larger volumes of ice core material for sampling.

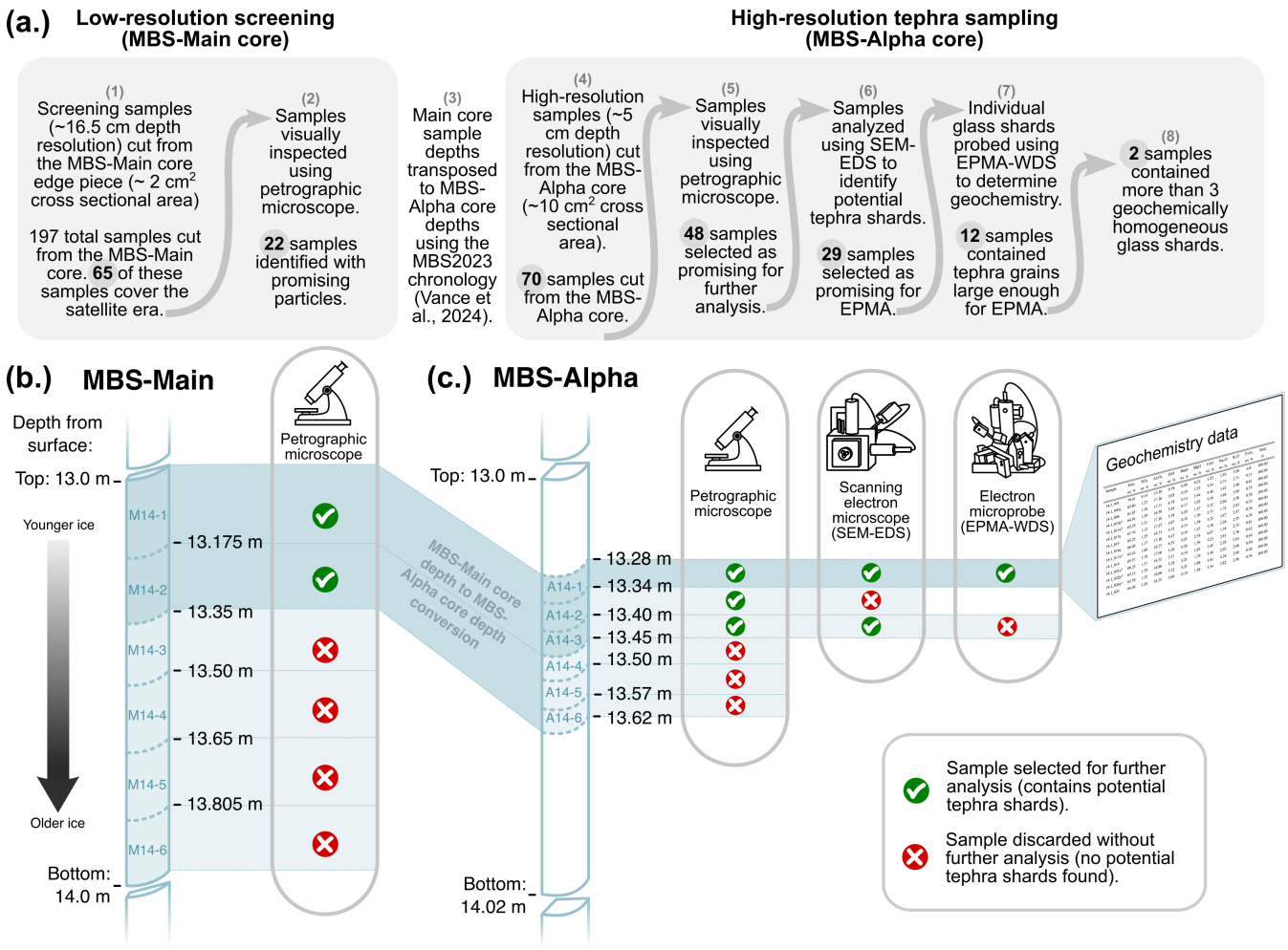

Figure 2. a. Schematic describing two-phase sampling strategy. A first low-resolution set of "screening samples" were prepared from the MBS-Main core, followed by a resampling from the MBS-Alpha core, due to larger available sample volume. Samples from the MBS-Alpha core were assessed based on visual examination using a petrographic microscope, scanning electron microscopy by energy dispersive spectroscopy (SEM-EDS) with automated mineralogy (AMICS), backscatter electron (BSE) imaging, and finally geochemistry was measured using electron probe microanalysis (EPMA). Examples shown of sampling procedure for selected samples from 13 - 14 m depth from the MBS-Main (b.) and MBS-Alpha (c.) cores.

2.2 Atmospheric circulation modeling

105 The Hybrid Single Particle Lagrangian Integrated Trajectory model (HYSPLIT; Stein et al. (2015)) was used in conjunction with the age-at-depth chronology for the Alpha ice core as a one element of our strategy for sample selection as well as to investigate potential sources of volcanic glass shards identified at the MBS site. Specifically, in sample planning, atmospheric

trajectories that were deemed favorable to transport of a specific event to the MBS site were identified, and provided an independent timestep to guide initial sampling. While atmospheric trajectory modeling is often used as a tool for validation of ice core cryptotephra correlations and deposition timing (Koffman et al., 2017; Evangelista et al., 2022; Lee et al., 2024), its implementation for targeted sampling is not well documented in the literature. Trajectories were used both to guide the sampling strategy and in the correlation of the cryptotephra horizons found in MBS-Alpha.

Guided by previous studies which have demonstrated the dominance of extreme precipitation events and atmospheric rivers on accumulation at the MBS site (Jackson et al., 2023; Wille et al., 2021; Maclennan et al., 2022), and the important role of meridional transport of maritime air masses in such extreme events (Jackson et al., 2023; Turner et al., 2022), we targeted transport from the Southern Indian Ocean using HYSPLIT trajectory analysis. To this end, daily 120-hour forward trajectories were computed, originating from 53.1°S 73.52 °E (central Southern Indian Ocean) from 1979 - present. Favorable transport conditions were identified by trajectories passing within 0.5°of the MBS site, and were used to assist with development of a directed sampling plan. Time periods with favorable trajectories were compiled together with volcanic signatures in the MBS ice chemistry record and known regional eruption events to prioritize the first pass of low-resolution sampling (six samples per meter) by aligning to the independent age-at-depth chronology developed for MBS-Main.

Trajectory analysis was additionally used in the validation of the tephra horizons identified here. Once potential horizons were identified, six-hourly ten day back trajectories were generated originating from 1500 m AGL at the MBS site (to avoid trajectories hitting the ground; Fig. 1). Frequency analysis of these trajectories was used in assessing the proposed tephra horizon correlations.

For ease of trajectory generation and repeatability, we used the PySPLIT package (Warner, 2018) for all trajectory generation. NCEP/NCAR reanalysis meteorology data (Kalnay et al., 1996) was used to drive the model. Individual trajectories were clustered using the built-in clustering algorithm in HYSPLIT. The aim of the algorithm is to identify a number of (user-defined) maximally distinct clusters while minimizing variability within each cluster (Stein et al., 2015).

Lagrangian transport models like HYSPLIT are some of the most commonly used tools for investigating particle atmospheric transport but should be considered with caution. As back trajectory timelines become longer (as in the case of the 10-day trajectories used here), the potential for error due to atmospheric noise introduced into the model increases. Despite the potential for the influence of such noise in the model systems, we find HYSPLIT to be useful as a confirmatory tool, used in parallel with geochemical analysis and existing satellite observations of volcanic ash transport.

2.3 Ice core sampling

For the first low-resolution screening process, sample depths were selected from MBS-Main based on atmospheric circulation modeling, in conjunction with known regional eruption records and volcanic signals in the ice core chemistry, in order to target volcanic material entrained in mid-latitude moisture from the southern Indian Ocean. These moisture-rich air masses were targeted using HYLSPLIT trajectory generation (as described in section 2.2), selecting for meridional transport trajectories, as it has been demonstrated that the meridional transport pathway is a source of significant snowfall accumulation to MBS (Jackson et al., 2023; Udy et al., 2021; Vance et al., 2024a). We hypothesize that air masses transported along these trajectory

lines could entrain material from volcanoes in the Kerguelen Plateau region (Heard and McDonald Islands) or from sources further afield. In order to refine our sampling strategy and to mitigate the need for time-consuming high-resolution sampling of the full length of the core, we targeted our screening sampling towards depth/ages that corresponded with air masses passing over the Kerguelen Plateau region (i.e. meridional transport) prior to arriving at MBS.

As this is the first investigation of cryptotephra in the MBS ice cores, for this study we focus on the satellite era (1979-present). This allows us to utilize atmospheric circulation modeling to assess volcanic ash transport, and to consider satellite volcanic observations to inform our volcanic matching efforts. Additionally, knowledge of the magnitude and timing of eruption events identified in satellite era ice cores can help fine-tune future efforts to reconstruct events identified from volcanic horizons in the more distant past. Furthermore, from a practical perspective, the duplicate cores covering this period allows for larger sample volumes for analysis, increasing the likelihood of capturing sparse tephra in a given sample.

First, a broad low resolution screening of the targeted depths was conducted from the MBS-Main core based on the previously described sampling plan and using samples ranging from 15-18 cm in length (six samples per one-meter-long ice core segment, Fig. 2b, measured to the nearest half-centimeter), and cut with a band saw from the outer edge of the core ($\sim$2 cm^2 cross sectional area). With a minimum annual layer thickness throughout the satellite era of 0.256 m firn depth (mean 0.501 $\pm$0.137 m, based on the MBS2023 chronology (Vance et al., 2024b)), this sample size represents at least sub-annual sampling resolution. MBS-Main core samples were melted in clean, new polycarbonate bottles before being transferred to clean new 10 ml centrifuge tubes and centrifuged (5 minutes, 3000 rpm). The resulting concentrate was evaporated on frosted glass slides and the remaining sample material was coated in low-viscosity epoxy resin (Logitech type 301 2-part epoxy resin). For efficiency and because of difficulties resulting from the preparation of the slides, these samples were only investigated using optical microscopy, and samples depths were prioritized based on the presence or absence of potential tephra grains. Of a total of 65 exploratory samples from the MBS-Main core, 22 samples were selected based on visual inspection using optical microscopy for re-sampling of the corresponding depth ranges in the MBS-Alpha core (Fig. 2a. 1-2).

As these samples were prepared from a narrow outer edge piece from the ice core, the small cross-sectional area meant that robust sample cleaning/decontamination procedures were not feasible for the MBS-Main samples. We were therefore not able to eliminate the potential for contamination by transfer from one core depth to another. General lab contamination debris also potentially obscured tephra and limited our ability to form robust identifications. Additionally, due to the sample preparation methods used for the MBS-Main samples (uneven surface of the glass slides used), we were not able to reliably fully section the very fine tephra grains for further microanalysis and were thus required to rely only on optical microscopy for these samples. This necessitated secondary sampling from the MBS-Alpha core, of which there was more sample volume remaining (Fig. 2c). The MBS-Main samples were valuable in guiding our sample selection for MBS-Alpha, allowing very efficient, targeted use of the core.

The second phase of sampling was able to be conducted at a higher resolution due to the available sample volume available from MBS-Alpha. The depths from the 22 selected MBS-Main core samples were transposed to the corresponding MBS-Alpha core depths (based on the annual horizons presented in Vance et al. (2024a), Fig. 2 a. 3), resulting in 70 sample depths ranging from 4-8 cm in length (Fig. 2a. 5). Samples were measured to the nearest half-centimeter and cut using a thin bladed pull-

saw. Careful decontamination procedures were followed during the cutting and preparation of the MBS-Alpha ice samples to prevent transfer of sample material from one sample to the next. MBS-Alpha samples were cut and decontaminated under a laminar flow hood in the cold lab. The cutting surface and blades were cleaned between each individual ∼5 cm sample, and both the ceramic blade used and the cutting surface (a clean, new plastic cutting board) were changed and washed with ultrapure water between samples from each meter of core (e.g. a freshly washed blade and cutting board were used for samples from MBS-Alpha 14, and then washed before decontamination of samples from MBS-Alpha 15).

After ∼1 mm of material from each of the outer edges was removed using a ceramic blade, the samples had a cross sectional area of ∼10 cm^2. Samples were melted at ambient temperature in rinsed sterile Whirl-Pak bags. Melted sample material was transferred to acid-washed 15 ml centrifuge tubes, and Whirl-Pak bags were rinsed at least twice with ultrapure water to minimize the possibility of sample material being left behind in the bags. Samples were then centrifuged (5 minutes, 3000 rpm) and the resulting concentrate was pipetted into wells created by placing cleaned 25 mm acrylic rings on polyimide (Kapton) tape adhered to flat glass plates, and set to evaporate on a hot plate at 60 °C. The centrifuge tubes were subsequently rinsed at least twice with ultrapure water, and the rinse water was added to the same sample area to evaporate. Each sample well was then backfilled with low-viscosity epoxy (Struers EpoFix) to create round resin mounts.

The sample mount surfaces were polished using 1 μm aluminum oxide polishing compound to remove surface resin and expose any tephra grains present in the mounts, then cleaned in an ultrasonic bath to remove excess polishing compound. Samples were examined using transmitted and reflected light using a petrographic microscope, and mounts identified as containing tephra grains of suitable size and quality for future electron probe microanalysis (EPMA; e.g. with large enough surface area for the EPMA beam accounting for mineral inclusions and/or vesicles; larger than ∼5 μm on the shortest axis. Fig. 2a. 6) were carbon-coated in preparation for BSE imaging, scanning electron microscopy by energy dispersive spectroscopy (SEM-EDS, FEI MLA 650 ESEM), and EPMA (2a. 7-9) at the Central Science Laboratory at the University of Tasmania.

2.4 Sub-annual age determination

While MBS annual layer thickness allows for sub-annual sampling, the site is characterized highly variable accumulation, both between- and within years (Vance et al., 2024a; Crockart et al., 2021; Jackson et al., 2023). Annuals in MBS-Alpha range 22.6 - 85.4 cm firn depth, and Jackson et al. (2023) found that 88% of inter-annual variability in MBS is associated with extreme precipitation, with on average ∼6% of days accounting for over 50% of annual accumulation.

No sub-annual chronology has been published for MBS, however Vance et al. (2024a) characterize the seasonality of impurity flux to the MBS site. Here, we rely on the austral summer peaking sulfate-to-chloride ratio (SO_4^{2-}/Cl^-) and $\delta^{18}O$ and austral winter peaking sodium (Na^+) (Vance et al., 2024b; Moy et al., 2024) to approximate within-year ages. We note, however, that such linear interpolation-derived sub-annual dating does not account for within-year variability, and therefore should be considered with caution.

2.5 Geochemical analysis of tephra

The mounted volcanic glass shards were analyzed using EPMA at the Central Science Laboratory (CSL) at the University of Tasmania (Fig. 2) in 2023 and early 2024. Analyses were conducted on a JEOL JXA-8530F Plus field emission microprobe with five wavelength dispersive spectrometers. Single point analyses used a 2 μm beam diameter with 4 nA beam current, 15 kV accelerating voltage. Analytical conditions were chosen to balance minimizing beam damage, particularly Na ion migration, while maintaining a beam size suitable for our smallest ($\leq$5 µm) shards.

EPMA analytical conditions were selected in collaboration with the instrument scientists, with the aim of obtaining as robust analytical totals as possible on our small glass shards while minimizing alkali ion migration and maintaining consistent analytical conditions across all measurements. While larger a beam size could have been used for a few of the larger samples analyzed using the broad-beam overlap method (Iverson et al., 2017), we chose to prioritize consistent analytical techniques, using the same beam size for all samples analyzed in order to enable better comparison across samples and obtain results from the largest number of glass shards possible in our samples.

Concentrations of 12 major and minor element oxides were measured in the individual shards (SiO_2, TiO_2, Al_2O_3, FeO, MnO, MgO, CaO, Na_2O, K_2O, P_2O_5, SO_3, F). A series of mineral standards were used for instrument calibration, a rhyolitic glass reference standard from the Smithsonian Institution Department of Mineral Sciences (VG-568, NMNH 72854; Jarosewich et al. (1980)) was used to validate accuracy and precision of measurements between measurement sessions. See Supplementary information for full details on the EPMA measurements and standards.

The dataset was detection limit filtered (99% confidence), and erroneous analyses of non-volcanic material (e.g. quartz grains or other mineral particles in the samples) were removed from the dataset. Data were corrected for Cl concentrations and normalized to 100% anhydrous as recommended by Iverson et al. (2017) prior to interpretation. Full geochemical results and secondary standards measurements can be found in the supplementary materials.

3 Results

Potential glass shards were identified in 48 out of the 70 samples prepared from the MBS-Alpha core using a petrographic microscope. Those 48 samples were inspected using BSE imaging and SEM-EDS with automated mineralogy at 5 μm resolution, and 29 were identified as containing glass shards selected for further analysis using EPMA. All samples contained relatively abundant material of non-volcanic origin, including mineral grains, diatom fragments, and infrequently, identifiable laboratory contamination (glove fibers, dust, etc.) The samples not selected for further analysis either contained mineral grains previously mis-identified (e.g. quartz) or grains too small or positioned too deep in the resin to have been appropriately sectioned in polishing. These 29 samples were analyzed with EPMA, producing reliable results for tephra grains in 12 of those 29 samples (Fig. 2). The 17 discarded samples contained grains with complex morphology (no surface large enough for reliable probe positioning), grains that had not been fully sectioned due to their size, or shards that were thin enough that the interaction volume of the probe beam included resin below the shard. A summary of all volcanic glass shards geochemically characterized in the MBS-Alpha core is reported in Table 1 and further discussion of analytical limitations is provided in Section 3.3.)

Table 1. Summary of the 12 MBS-Alpha ice core samples containing volcanic glass shards analyzed by EPMA-WDS. Sample depths were measured to the nearest half-centimeter from the top of each ice core segment during sampling in the freezer laboratory and assimilated with core top depths; measurement error associated with core length estimates are in line with information provided in Vance et al. (2024a). Ages provided here are approximated based on MBS2023 chronology (Vance et al., 2024a). Composition classifications are based on total alkali-silica (TAS) diagram (Le Bas et al., 1986), the number of shards of each composition is given in parentheses. Further discussion of proposed volcanic sources (bold text in table) can be found in section 4.

Sample ID	Sample depth range	Approx. date	Total shard count	Composition *(Le Bas et al., 1986)*	Proposed source
7-6	6.39-6.45 m	Mid 2004	3	Phonolite (1), Dacite (2)	-
7-7	6.45-6.51 m	Mid 2004	1	Rhyolite (1)	-
8-5	7.98-8.05 m	Mid 2001	3	Rhyolite (3)	-
9-10	8.94-9.00 m	Early 2000	3	Rhyolite (1), Dacite (1), Basaltic Andesite (1)	-
13-3	12.79-12.85 m	Mid 1992	1	Rhyolite (1)	-
14-1	**13.28-13.34 m**	**Mid 1991**	**13**	**Dacite (12), Andesite (1)**	**Cerro Hudson**
16-4	15.93-16.00 m	Early 1987	2	Rhyolite (2)	-
17-1	16.00-16.045 m	Early 1987	1	Rhyolite (1)	-
17-5	16.20-16.25 m	Mid 1986	1	Trachyte/Trachydacite (1)	-
17-9	**16.87-16.915 m**	**Mid 1985**	**10**	**Phonolite (10)**	**Mt. Erebus**
18-1	17.00-17.05 m	Mid 1985	1	Trachyandesite (1)	-
18-5	17.24-17.30 m	Early 1985	3	Trachyandesite (1), Trachyte/Trachydacite (1), Rhyolite (1)	-

3.1 Tephra morphology

Glass shards are most abundant in the 13.28-13.34 and 16.87-16.915 m depth samples. The 13.28-13.34 m sample has the largest glass shards (Fig. 3), ranging from 10-20 μm along the longest axis. All shards are angular, while the larger shards in this sample have cuspate, bubble-wall, or y-junction morphologies and smaller shards appear more blocky or platy. Glass shards in the 16.87-16.915 m sample are typically smaller, <10 μm, with only one shard <10 μm ($\sim$15 μm) across the longest axis. These shards have simpler angular morphology, and include blocky and platy shapes, some have fluted or cuspate edges. The remaining samples contain glass shards ranging from <5 to 15 μm, with mostly simple angular morphologies.

Table 2. Major element oxide concentrations of volcanic glass shards identified in the MBS-Alpha core. Symbols correspond with the legend in Figure 4. Analyses were conducted on a JEOL JXA-8530F Plus field emission microprobe with five WDS spectrometers. Single point analyses used a 2 μm beam diameter with 4 nA beam current, 15 kV accelerating voltage. Data are normalized to 100% using the Cl-adjusted analytical total, following the "broad beam overlap" method introduced in Iverson et al. (2017). "n.d." indicates measured values below instrument detection limit. For shards with multiple point measurements, average of measurements is indicated by "a" in sample name, and n indicates number of points measured per shard.

Sample		SiO_2	TiO_2	Al_2O_3	FeO	MnO	MgO	CaO	Na_2O	K_2O	P_2O_5	Total	n
		wt. %	wt. %	wt. %	wt. %	wt. %	wt. %	wt. %	wt. %	wt. %	wt. %	%	
7-6_002*	×	66.16	0.09	20.07	1.00	n.d.	0.14	4.94	6.53	0.69	0.11	100.00	1
7-6_013	×	65.13	1.63	14.78	8.61	n.d.	0.47	2.55	5.44	0.98	0.32	100.00	1
7-6_014	×	59.08	0.99	19.51	4.27	0.23	0.81	1.34	7.61	5.50	0.29	100.00	1
7-7_006	+	77.16	0.30	13.11	0.22	n.d.	0.17	0.94	2.06	6.00	0.00	100.00	1
8.5_005	●	77.31	0.13	13.11	0.40	0.06	0.07	0.51	3.96	4.49	0.03	100.00	1
8.5_007*	●	77.10	0.04	13.18	0.43	n.d.	0.00	0.48	4.36	4.36	0.05	100.00	1
8.5_010	●	73.97	0.34	14.60	1.43	n.d.	0.43	1.53	3.22	4.51	0.06	100.00	1
9-10_014	▲	56.70	1.12	21.70	7.56	n.d.	2.20	5.13	2.58	2.53	0.43	100.00	1
9-10_017	▲	75.26	0.08	15.38	0.47	n.d.	0.40	0.19	6.71	1.47	0.00	100.00	1
9-10_021	▲	67.32	0.39	12.13	8.00	0.17	6.83	1.47	1.44	2.08	0.15	100.00	1
13-3_011	▼	69.48	0.59	15.77	2.65	n.d.	0.85	2.64	3.43	4.29	0.13	100.00	1
14-1_003a	✸	65.80	1.27	17.16	5.05	0.19	1.53	3.24	2.73	2.71	0.31	100.00	2
14-1_006	✸	61.87	1.38	17.31	6.19	0.14	2.44	4.48	3.42	1.99	0.61	100.00	1
14-1_010a	✸	64.91	1.29	16.59	5.45	0.17	1.82	3.30	3.46	2.60	0.35	100.00	3
14-1_011a	✸	65.35	1.31	17.10	5.38	0.20	1.47	3.32	2.90	2.58	0.38	100.00	2
14-1_013a	✸	67.79	1.12	17.27	4.67	0.16	1.39	2.77	1.74	2.83	0.32	100.00	2
14-1_015	✸	65.23	1.25	16.73	5.15	0.15	1.59	3.25	3.67	2.57	0.36	100.00	1
14-1_016a	✸	66.05	1.17	17.16	5.47	0.18	1.47	3.39	2.26	2.55	0.36	100.00	2
14-1_017a	✸	63.43	1.60	16.77	6.52	0.21	2.34	4.67	1.38	2.33	0.61	100.00	2
14-1_019	✸	65.57	1.19	17.00	5.26	0.20	1.58	3.23	2.61	2.76	0.42	100.00	1
14-1_021a	✸	66.23	1.31	16.72	5.21	0.19	1.65	3.45	2.28	2.63	0.40	100.00	2
14-1_022a	✸	65.15	1.30	16.86	5.28	0.21	1.70	3.38	2.92	2.66	0.50	100.00	2
14-1_024a	✸	63.76	1.32	16.69	5.52	0.21	1.69	3.41	4.28	2.60	0.49	100.00	2
14-1_025	✸	64.48	1.20	16.75	5.60	0.19	1.59	3.34	3.82	2.56	0.34	100.00	1
16-4_014	▶	76.90	0.06	13.77	0.42	0.10	0.07	0.48	3.75	4.36	n.d.	100.00	1

continued on following page

continued from previous page

Sample		SiO_2 wt. %	TiO_2 wt. %	Al_2O_3 wt. %	FeO wt. %	MnO wt. %	MgO wt. %	CaO wt. %	Na_2O wt. %	K_2O wt. %	P_2O_5 wt. %	Total %	n
16-4_024	▶	73.11	0.03	16.05	2.50	0.04	0.02	0.68	3.22	4.34	n.d.	100.00	1
17-1_014	◀	75.83	0.13	18.81	0.72	n.d.	0.33	0.67	3.06	0.28	0.02	100.00	1
17-5_081*	■	61.27	0.14	25.36	1.26	n.d.	n.d.	1.78	6.25	3.92	0.00	100.00	1
17-9 _005	★	57.02	1.01	20.14	5.04	0.27	0.99	1.91	7.88	5.22	0.26	100.00	1
17-9 _008	★	58.76	0.97	19.97	3.99	0.13	0.80	1.00	8.87	5.11	0.29	100.00	1
17-9 _009*	★	57.10	0.98	19.80	5.81	0.20	0.97	1.80	7.04	5.76	0.31	100.00	1
17-9 _010	★	57.32	1.03	19.68	5.30	0.29	0.86	1.92	7.69	5.49	0.32	100.00	1
17-9 _011	★	56.48	0.98	20.16	4.73	0.31	0.93	1.76	9.12	5.11	0.25	100.00	1
17-9 _013	★	56.44	1.09	20.06	5.64	0.33	0.92	1.85	8.10	5.19	0.29	100.00	1
17-9 _018	★	57.38	0.90	20.12	5.04	0.20	0.96	1.68	8.56	4.87	0.18	100.00	1
17-9 _019	★	56.31	1.06	20.01	5.18	0.25	0.87	1.95	8.46	5.32	0.28	100.00	1
17-9 _020	★	57.64	0.93	19.94	4.83	0.25	0.84	1.67	8.73	4.78	0.22	100.00	1
17-9 _032	★	56.86	1.04	20.09	5.18	0.31	0.86	1.76	8.24	5.25	0.23	100.00	1
18-1_014	⊙	51.70	2.94	14.15	11.16	0.16	3.09	7.72	4.38	3.72	0.94	100.00	1
18-5_004	◆	65.13	0.12	20.50	0.22	n.d.	0.00	1.82	8.32	3.97	n.d.	100.00	1
18-5_013	◆	72.81	0.39	15.29	1.76	0.17	0.38	1.10	4.08	4.12	n.d.	100.00	1
18-5_020*	◆	53.09	1.03	18.21	13.84	2.37	0.54	4.28	5.06	0.55	0.86	100.00	1

"a" indicates values averaged over multiple analyses on a single glass shard; * indicates analytical totals below 60%.

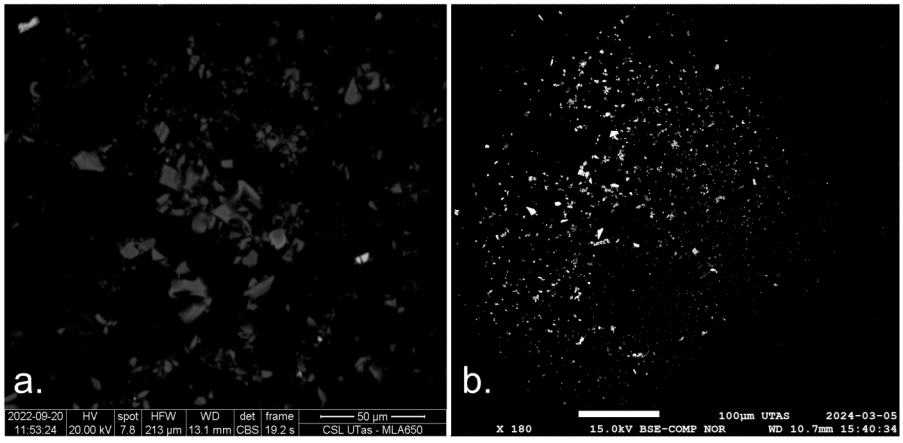

Figure 3. Example backscatter electron images of sample material found in the MBS-Alpha core in the 13.28-13.34 m (a) and 16.87-16.915 m (b) samples.

3.2 Geochemical composition

Major element oxides of all tephra identified in the MBS-Alpha core are provided in Table 2. The MBS-Alpha glass shards have SiO_2 values ranging from 51.70 to 77.31 wt.%, with 1.38-9.12 wt.% Na_2O, and 0.28-6.0 wt.% K_2O (Fig. 4, Table 2). When plotted on the TAS diagram (Le Bas et al., 1986), compositions for the glass shards include basaltic andesite, trachyandesite, andesite, dacite, trachyte/trachydacite, rhyolite, and phonolite. The most abundant compositions are dacite (15 shards), phonolite (11 shards), and rhyolite (10 shards). Remaining compositions have fewer shards (one basaltic andesite, two trachyandesite, one andesite, and two trachyte/trachydacite shards).

The glass shards in the 13.28-13.34 m sample (Table1) are mainly dacite in composition, with one andesite shard (Fig. 4). The analyses from this depth have SiO_2 ranging from 61.87 to 66.23 wt.%, with total alkalis (Na_2O+K_2O) ranging from 3.16 to 7.27 wt.%. Bivariate diagrams demonstrate there is little variation in the abundance of other major element oxides when plotted against SiO_2 (Fig. 4).

All glass shards analyzed in the 16.87-16.915 m sample (Table1 have a homogeneous phonolitic composition. Compared to the 13.28-13.34 m horizon, these glass shards have a somewhat lower SiO_2 concentration, ranging from 56.31 to 58.76 wt.% and are strongly alkaline (Na_2O+K_2O), ranging from 12.80 to 14.23 wt.% (Fig. 4). As a group, these shards have among the highest Na_2O and K_2O contents of all MBS-Alpha glass analyzed here (7.04-9.12 and 4.78-5.76 wt.%, respectively).

3.3 Analytical limitations

EPMA analytical conditions were selected and analyses completed prior to the publication of the recommendations for best practices for EPMA analysis of fine grained tephra (Innes et al., 2024). Our analytical conditions produced meaningful results, however some limiting aspects require consideration.

Many of the analyses have analytical total oxide values of >90%, due to the very small size of the shards (<5μm). However, approximately half of the sample analyses resulted in lower analytical totals. Of the 42 EPMA data measurements presented here, five have analytical totals below 60% (indicated in Table 1). We attribute low analytical totals to the following scenarios (1) glass shards that are very thin (either naturally, or due to the amount of polishing required), resulting in an interaction volume depth that includes the resin substrate below the shards and/or (2) larger shards with complex morphology causing the resin to be not uniformly removed from the surface of the shards, resulting in some resin being included in the beam area. This could have been resolved by additional polishing, however this risked fully polishing away some of the smaller shards in the sample. As a result, we chose to accept slightly lower totals in order to include analyses of as many shards as possible.

Iverson et al. (2017) show with their "broad beam overlap" method that analytical totals as low as 67% are statistically similar to the same analyses with higher analytical totals, with only a slight decrease in precision. Narcisi et al. (2019) show reliable results with analytical totals as low as 60%. Innes et al. (2024) report good accuracy despite somewhat lower precision for EPMA analyses of very fine grained tephra shards resulting in analytical totals ranging from as low as 35% up to 101 wt.%. Following this approach, analyses with analytical totals of at least 50% are presented here. Only one sample with <60% total

(shard 17-9_009) is included in the horizons that we pursue source correlations for. As the major element compositions of this shard fall within the range of the other glass shards in this sample, we have chosen to include it in our analyses.

The probe beam used in EPMA has the potential to damage the sample by inducing migration of alkali ions (typically Na_2O; Gedeon et al. (2000); Humphreys et al. (2006); Kuehn et al. (2011)). Analytical conditions for EPMA were selected to minimize potential migration of alkali ions for small glass shards and repeated analysis of secondary standards did not show a loss of sodium over time (see supplementary materials). This loss of sodium is due to probe beam damage in cases of repeated analysis in a small area or single glass shard. While most of the glass shards in our sample were too small to fit multiple analyses, some of the glass shards in the 13.28-13.34 m sample were large enough for multiple analyses. Data from these analyses are presented in Table 2 as the average of multiple analyses (see supplement for individual point measurements). Some of these glass shards did show decreases in Na_2O over multiple analyses (see Figure S.1 in supplementary materials) and consequently we have not relied exclusively on Na_2O values for our tephra source identification.

3.4 Sample age estimates

The 13.28-13.34 m sample falls between the 1991 and 1992 annual horizons (13.761 and 13.099 m respectively, MBS2023; Vance et al. (2024a)). In Figure 5, sample depth ranges are shown alongside seasonally varying isotope and chemistry species measured in the MBS-Alpha core. It is notable that during the development of the MBS2023 chronology, it was determined that trace chemistry was as reliable as $\delta^{18}O$, and at times more so, in determining annual horizon positions in the MBS records (see section 4.3 in Vance et al. (2024a)). It can be seen in Figure 5 that the 13.28-13.34 m sample falls towards the end of the austral winter sodium peak, but just at the start of the austral summer peak in sulfate-on-chloride, indicating that the glass shards were likely deposited with snow that fell in mid to late 1991. It can also be seen that the sample falls just at the beginning of a significant peak in non-sea-salt sulfate, likely volcanic in origin.

The 16.87-16.915 m sample falls between the 1985 and 1986 annual horizons (17.282 and 16.679 m respectively). This sample depth coincides with the end of the austral winter sodium peak and the start of the the sulfate-on-chloride peak, indicating that this sample likely represents snow from the middle of the year (late austral winter to early spring) 1985.

For clarity, we will hereafter refer to these two samples by their year of origin, according to the MBS2023 chronology; 1991 for the 13.28-13.34 m sample, and 1985 for the 16.87-16.915 m sample.

4 Volcanic source identification

The majority of tephra-bearing sample depth ranges from MBS-Alpha contain sparse and/or heterogeneous tephra shard compositions. However, when plotted on the TAS diagram (Le Bas et al., 1986), the 1991 and 1985 samples contain abundant glass shards (13 and 10 shards respectively), each with largely homogeneous compositions (Fig. 4). We therefore consider these two samples as discrete cryptotephra horizons in the MBS-Alpha core. The remaining samples each contain three or fewer glass shards. Some of these samples do cluster together across sample depths (e.g. cluster of rhyolitic deposits, Fig. 4), however as these shards comprise a wide range of ice core depths, they cannot be correlated as the product of a single eruption event. As

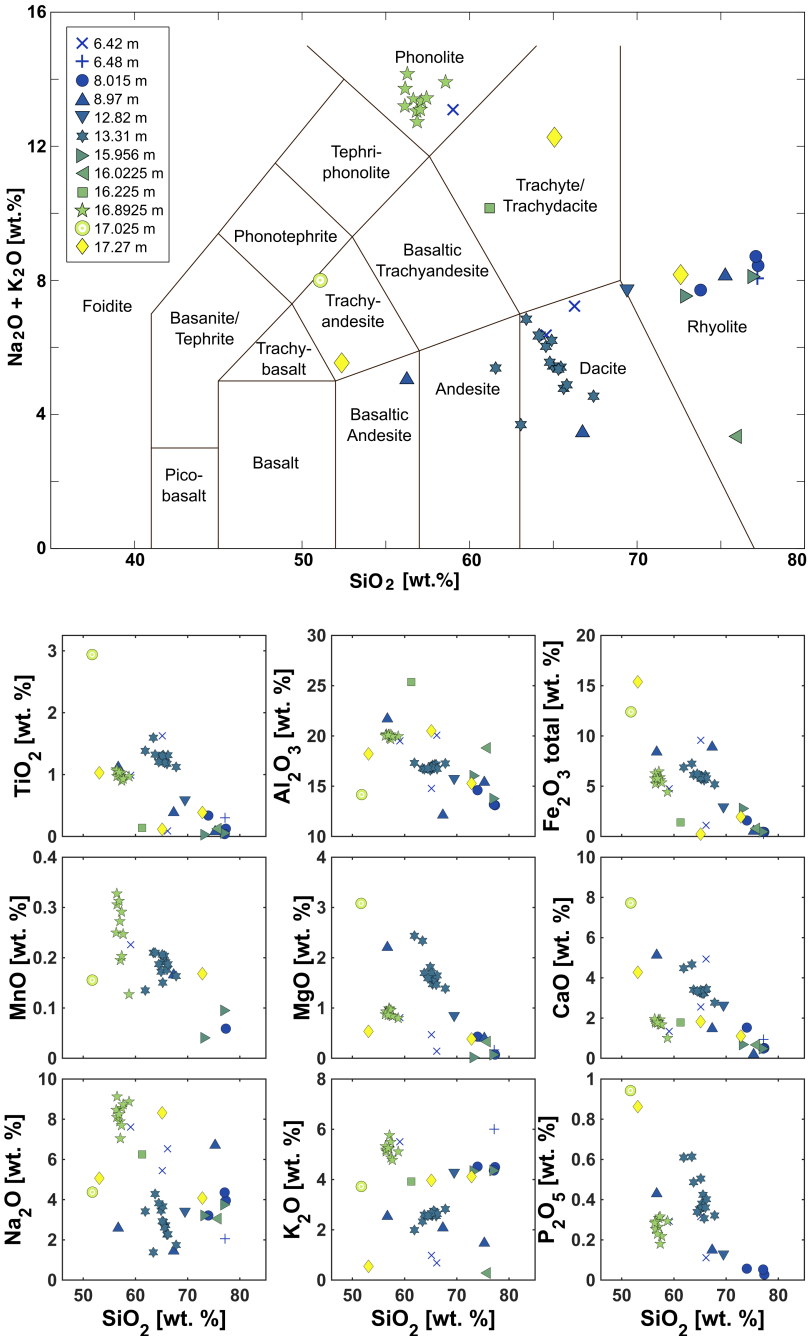

Figure 4. Total alkali-silica (TAS, Le Bas et al. (1986)) diagram and variation diagrams for all individual glass shards identified in the MBS-Alpha core. Data are normalized to 100% (anhydrous) using the Cl-adjusted analytical total, after Iverson et al. (2017).

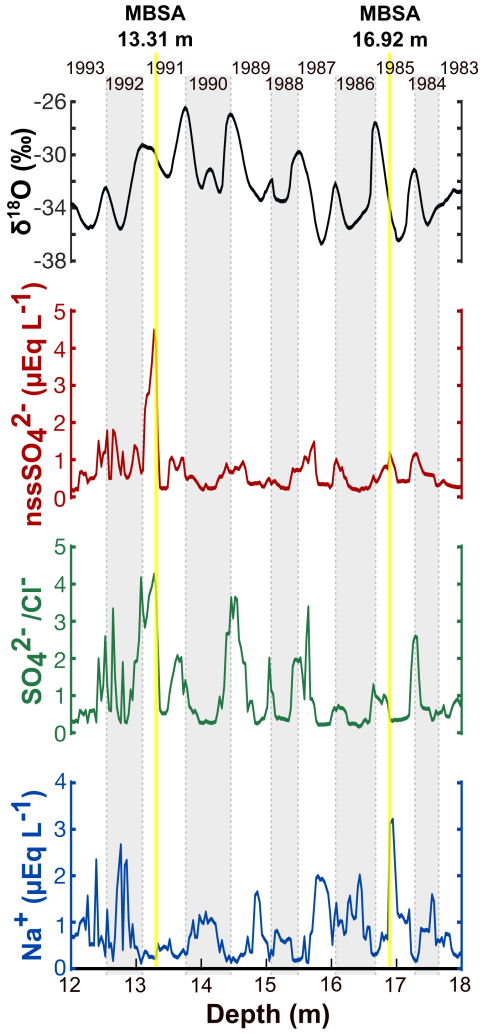

Figure 5. Selected seasonally varying glaciochemical species (nssSO_4^{2-}, calculated using the measured Na^+ to remove the sea salt sulfate component, following Plummer et al. (2012), ratio of sulfate to chloride (SO_4^{2-}/Cl^-), and sodium (Na^+)) and isotope ($\delta^{18}O$) measured from the MBS-Alpha core with tephra horizon depths indicated (yellow bars). Annual horizons (MBS2023 January 1 year boundaries, after Vance et al. (2024a)) indicated by vertical dashed lines.

none of the remaining samples (aside from the 13.28-13.34 m and 16.87-16.915 m horizons) include more than three shards, for this study, we primarily focus our source attribution efforts on groups with more than three shards of similar composition to ensure reliable correlations (similar to the approach taken by Cook et al. (2022)).

4.1 Rhyolite group

A small number of shards originating from a range of sample depths (from 6.48 to 17.27 m depth), form a compositionally similar group of rhyolites. Despite originating from a broad range of depths (and therefore ages), if treated as a group, the composition of these shards cluster together across most major element oxides (Fig. 4). The composition of this cluster is similar to compositions determined for volcanic glass shards produced in the 1991 eruption of Pinatubo (Luhr and Melson, 1996; Tamura and Nakagawa, 2023). However none of the depths where glass shards of this composition were found correspond within reasonable dating error to the 1991 eruption of Pinatubo, where a sulfate peak is often used as a dating horizon for 1991/1992 in other ice cores (Plummer et al., 2012; Crockart et al., 2021; Vance et al., 2024a).

The rhyolitic glass shard compositions fall within the range of compositions of sparse mid- to late-Holocene rhyolite shards reported in the B53 and B54 ice cores, which Abbott et al. (2024) correlate with shards identified in the Talos Dome ice core. Narcisi et al. (2012) attribute these Talos Dome rhyolite shards to various extra-Antarctic sources (including Andean and New Zealand sources). Del Carlo et al. (2018) have correlated similar high-K rhyolites with either "extremely evolved" products of West Antarctic intraplate volcanoes (including McMurdo group and Marie Byrd Land volcanoes, not active during the satellite era), but also show similarities to Antarctic samples correlated with South American (Aguilera) as well as South Shetland Islands volcanoes. Additionally, these rhyolites also show some compositional similarity to the rhyolitic component of a sample of ash collected from the crater rim of Mt. Erebus in 2000 (Silaev et al., 2020). Due to the multiplicity of sources attributed to tephra with similar compositions, as well as their sparseness in the MBS-Alpha core, we cannot confidently attribute a single source to this compositional group of rhyolites.

An alternative interpretation of such sparse and heterogeneous samples is to suppose they represent a fraction of the background "dust" signal often seen in ice core analyses (Plunkett et al., 2020; Hutchison et al., 2024; Vallelonga and Svensson, 2014; Delmonte et al., 2013). This background signal could include re-mobilized volcanic ash from a variety of sources, transported from nearby ice-free areas or other extra-Antarctic sources (Delmonte et al., 2013). Typically volcanic glass shards transported by wind display evidence of reworking e.g. abraded margins (Dunbar et al., 2003). Textural alteration depends on the duration and conditions of erosion and weathering glass shards are exposed to. While all glass shards chosen for analysis have angular shard-like morphologies that we interpret to be primary textures (see supplementary materials figure S.2 for an example BSE image of the 8.015 m sample), we cannot rule out the possibility that these glass shards come from re-mobilized material.

While robust contamination preventative precautions were taken during sampling, there is some possibility that some of these unidentified rhyolites (as well as the other unidentified sparse glass shards) could have been the result of contamination from unknown lab sources or between samples. We cannot definitively rule out this as a possibility, however we consider it unlikely, as the sparse shards have been characterized as tephra both based on visual inspection and geochemical composition, and all sample-contact surfaces were rigorously cleaned between preparation of each sample.

4.2 1991 Horizon

The presence of a substantial spike in nssSO_4^{2-} (Fig. 5, Vance et al. (2024b)), likely of volcanic origin, co-occurring with the 1991 sample bearing multiple glass shards suggests that the tephra found could be associated with the volcanic event that produced the sulfate signal in the ice core. Based on the age of the sample, we consider the two primary candidates for the source of the 1991 tephra horizon to be the eruptions of Pinatubo (Philippines, volcanic explosivity index (VEI) 6) and Cerro Hudson (Chile, VEI 5), both occuring in mid-1991 (Global Volcanism Program, 2024). However we also investigate all other significant (VEI 3 or greater) known tropical and Southern Hemisphere eruptions from 1991 (Nyamulagira, Democratic Republic of Congo and Lokon-Empung, Indonesia). Additionally, we include other Antarctic and sub-Antarctic volcanic sources (Gaussberg, South Sandwich Islands, and South Shetland Islands), as although there are no known eruptions of these volcanoes during 1991, they are known or speculated possible sources of tephra (primary or reworked) identified in other Antarctic ice cores (Geyer et al., 2023; Narcisi and Petit, 2021).

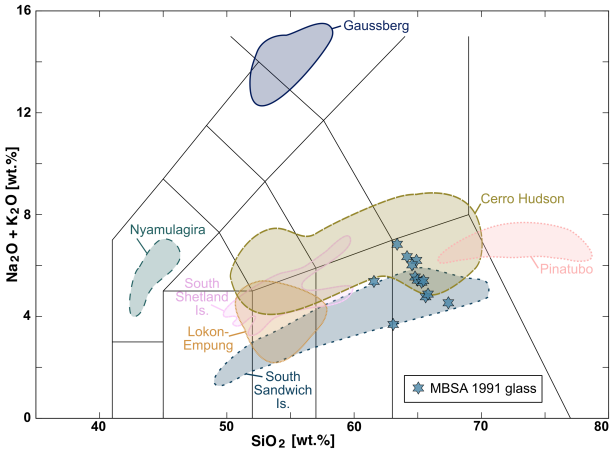

Figure 6. Total alkali-silica diagram (Le Bas et al., 1986) showing the MBS-Alpha 1991 glass together with representative data for possible eruption sources: Holocene products of Cerro Hudson (Haberle and Lumley, 1998), Nyamulagira (Aoki et al., 1985), Lokon-Empung (Dmitrieva et al., 2023), Gaussberg (Salvioli-Mariani et al., 2004), Pinatubo (Luhr and Melson, 1996; Tamura and Nakagawa, 2023), South Sandwich and South Shetland Islands (Narcisi et al. (2005), and references therein).

It is clear from the TAS diagram (Fig. 6) that products of Nyamulagira and Lokon-Empung do not correlate with glass from the MBS-Alpha 1991 horizon, and neither do the products of Gaussberg or the South Shetland Islands. We therefore rule these out as potential sources. While the South Sandwich Islands do appear to correlate somewhat better on the TAS diagram, when compared with literature values (Fig. 6; Abbott et al. (2024); Pearce et al. (1995)), the 1991 tephra is characterized by significantly higher K_2O values (1.99-3.09 wt.%) than South Sandwich Islands (<1.5 wt.% K_2O) for similar SiO_2 ranges. This combined with the lack of recorded eruptions of the South Sandwich Island volcanoes during this time period, leads us to rule out South Sandwich Islands as a potential source.

We are left with Pinatubo (June 15, 1991), and Cerro Hudson (August 8-14) as potential sources for the glass in the MBS-Alpha 1991 horizon. While we are able to approximate general sub-annual ages of the individual samples, due to the intra-annual variability seen in MBS accumulation (see section 2.4), the two-month difference between the Pinatubo and Cerro Hudson eruptions is below our ability to resolve based on dating uncertainty and the size of the sample ($\sim$6 cm). Since we cannot rely on sample age, we focus on geochemistry and atmospheric transport modeling to guide our source identification. The products of the 1991 eruption of Pinatubo are primarily rhyolitic (Fig. 7), and have much lower TiO_2 ($<$0.52 wt.%) and FeO ($<$3.01 wt.%; (Luhr and Melson, 1996; Tamura and Nakagawa, 2023)) than both the MBS-Alpha 1991 glass and the majority of the Cerro Hudson products. Based on the difference in TiO_2 and FeO, we rule out Pinatubo as a potential source candidate for the dacite cluster in the 1991 tephra. The geochemical compositions of the glass shards in the 1991 sample show a strong similarity to the Holocene volcanic products of the Cerro Hudson volcano (Fig. 7).

The 1991 eruption of Cerro Hudson was one of the 20th century's largest explosive eruptions, producing 43 km^3 (bulk volume) of tephra (Kratzmann et al., 2009). Beginning with a phreatomagmatic event on August 8, 1991, with a VEI of 3. A second phase of the eruption began on August 12 with a Plinian eruption with VEI of 5, which produced the majority of the tephra ejected during the eruption (Kratzmann et al., 2009, 2010b). The eruption ejected ash as high as >18 km into the stratosphere, and ash dispersal was well documented spanning thousands of kilometers to the southeast (Doiron et al., 1991; Constantine et al., 2000; Kratzmann et al., 2010b).

The major elements of the 1991 dacite tephra match well with Holocene volcanic products of Cerro Hudson (Fig. 7; variation diagrams against MgO included in supplementary materials, Figure S.3). This is seen particularly with the later products from the 1991 eruption, as the composition shifted from basaltic-andesite towards large volumes of trachyandesite to rhyo-dacite products (Fig. 7,Wilson et al. (2011); Naranjo S. et al. (1993); Kratzmann et al. (2009)). The dacite glass from the 1991 tephra horizon show a slightly less alkaline composition than some Cerro Hudson products, including glass shards from the 1991 eruption recovered from visible tephra deposits in lake and terrestrial cores from southern Chile (Streeter et al. (2024), Fig. 7). This lower alkalinity is driven largely by a lower concentration of Na_2O, while the remaining major element oxides show similar concentrations to the reported literature values for Cerro Hudson eruption products (Fig. 7; Fernandez and Bitschene (1993); Haberle and Lumley (1998); Gutiérrez et al. (2005); Kratzmann et al. (2009); Del Carlo et al. (2018); Panaretos et al. (2021); Abbott et al. (2024); Streeter et al. (2024)). The lower Na_2O value could be in part due to the minimal migration of sodium during EPMA analysis described in section 3.3 above. Despite the potential Na_2O loss, the majority of our analyses are within the range of concentrations of major element oxide concentrations seen in the literature for Cerro Hudson (Fig. 7). Based the geochemistry and chronology of this cryptotephra horizon, we propose that the MBS-Alpha 1991 tephra originate from the 1991 eruption of Cerro Hudson.

4.2.1 1991 Horizon: Sulfate and tephra deposition timing

The sample depth of the 1991 tephra horizon coincides with the start of a significant increase in the nss-SO_4^{2-} chemistry of the MBS-Alpha core (Fig. 5). It is common in ice core tephra studies to see a tephra layer deposited before the corresponding peak in nss-SO_4^{2-} (Burke et al., 2019; Koffman et al., 2013). The delay between deposition of volcanic ash and volcanic-

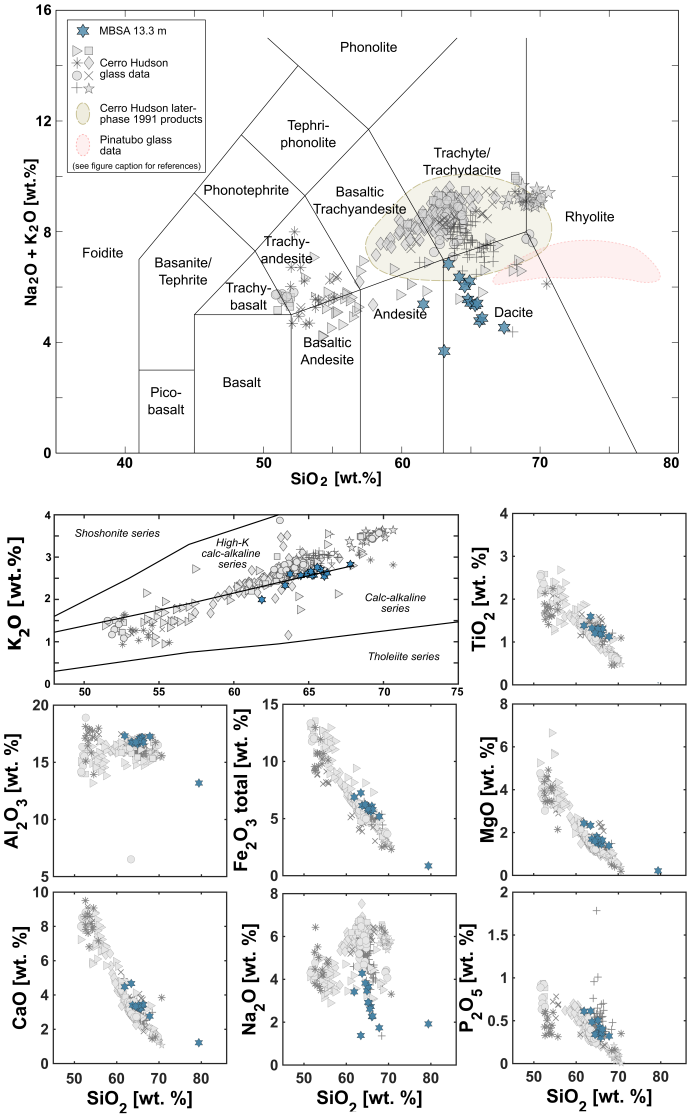

Figure 7. Total alkali-silica diagram (Le Bas et al. (1986)) and individual major element variation diagrams showing the 13.3 tephra horizon from MBS-Alpha (teal hexagram), together with literature values from various Holocene eruptions of Cerro Hudson (grey circles (Fernandez and Bitschene, 1993), triangles (Haberle and Lumley, 1998), crosses (Gutiérrez et al., 2005), squares (Kratzmann et al., 2010a), plusses (Del Carlo et al., 2018), stars (Panaretos et al., 2021), asterisks (Abbott et al., 2024), and diamonds (Streeter et al., 2024)). Green shaded area indicates characteristic compositions of volcanic products from only the later phase of the 1991 eruption of Cerro Hudson (Naranjo S. et al., 1993; Wilson et al., 2011; Kratzmann et al., 2009). Pink shaded area indicates characteristic compositions of volcanic glasses from the 1991 eruption of Mt. Pinatubo (Luhr and Melson, 1996; Tamura and Nakagawa, 2023). Discrimination lines on K_2O diagram after Peccerillo and Taylor (1976).

produced sulfate is variable, based on a combination of distance from the source volcano, scale and plume height of eruptive event, atmospheric transport conditions (Abbott et al., 2024; Plunkett et al., 2023; Koffman et al., 2017; Burke et al., 2019), as well as potential diffusion within the ice (Rhodes et al., 2024). A peak in sulfate that occurs without substantial lag following tephra deposition may indicate more rapid tropospheric transport and shorter residence time of sulfate aerosols, however the relationship is complicated in cases of long range transport from tropical eruptions (Plunkett et al., 2023). For the 520 BCE HW_6 eruption of Cerro Hudson, Abbott et al. (2024) identified a time lag of less than one year between elevated microparticle levels (indicative of volcanic ash/tephra deposition) and the peak in sulfate deposition in the East Antarctic Plateau B53 ice core.

In the case of the 1991 horizon, however, the sulfate spike is assumed to be a combined signal from both the Pinatubo eruption (June 12-15, 1991) and the Cerro Hudson eruption (August 8-15, 1991). The 1991 eruption of Pinatubo ejected an approximated 18 - 20 megatons of SO_2 into the atmosphere (Guo et al., 2004; Pitts and Thomason, 1993), the Cerro Hudson eruption two months later only produced an estimated 1.5 - 4 megatons of SO_2 (Doiron et al., 1991; Constantine et al., 2000; Case et al., 2024). The SO_2 produced in volcanic eruptions is oxidized through atmospheric processes, becoming SO_4^{2-} before deposition onto the snow surface, where it is measurable in the ice core (Burke et al., 2019). The order-of-magnitude greater SO_2 injection from Pinatubo prevents us from being able to disentangle the Hudson SO_2 signal from bulk ice core measurements without analysis of sulfur isotopes (Burke et al., 2019). Despite the difference in SO_2 injection, the Cerro Hudson eruption is estimated to have produced a slightly larger volume of tephra-fall deposits than Pinatubo: 2.7 km^3 and 1.8 - 2.2 km^3 dense-rock equivalent, respectively (Guo et al., 2004; Paladio-Melosantos et al., 1996). It is not uncommon for multiple peaks to be seen in ice core sulfate measurements in years following a major eruption, which can be due to seasonal deposition of sulfate or confounding eruptions (Legrand and Wagenbach, 1999; Guo et al., 2004). Due to the confounding sulfate signals, however, without sulfur isotopic measurements, interpretation of the time-lag between Cerro Hudson tephra deposition and bulk sulfate spike is not possible.

4.2.2 1991 Horizon: Atmospheric circulation

Because the ash dispersal and sulfate aerosol cloud produced by the 1991 eruption of Cerro Hudson has been well studied (Doiron et al., 1991; Schoeberl et al., 1993; Constantine et al., 2000; Kratzmann et al., 2010b; Evangelista et al., 2022; Case et al., 2024), we are able to use the observed atmospheric transport of Cerro Hudson ash in addition to HYSPLIT trajectory modeling. Use of infrared advanced very high resolution radiometer (AVHRR) and total ozone mapping spectrometer (TOMS) satellite data was used to investigate the volcanic ash and sulfate aerosol distribution, respectively, resulting from the 1991 Cerro Hudson eruption (Doiron et al., 1991; Constantine et al., 2000; Carn et al., 2003). The majority of the ash cloud produced during the Cerro Hudson eruptions was injected near the tropopause, and 90% of the ash cloud was observed to have settled out within a few days (Constantine et al., 2000). AVHRR data show that some part of the ash cloud was detected as far as Australia within five to six days of the August 15 eruptive phase (Constantine et al., 2000). AVHRR images from 18 August, 1991 show part of the Cerro Hudson volcanic ash cloud positioned over the Kerguelen Plateau, north of the MBS site, lying

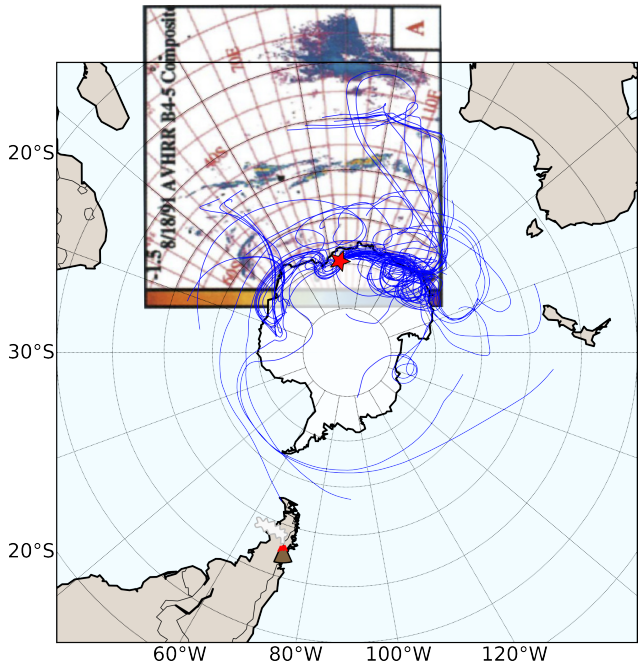

Figure 8. Map showing ten-day back trajectories originating every six hours (44 total trajectories) from the MBS site (indicated by red star), from 12 to 22 August, 1991. Inset AVHRR figure shows the location of the Cerro Hudson ash cloud on 18 August, 1991. Cerro Hudson indicated by volcano symbol. (AVHRR figure from Constantine et al. (2000)).

along the 50°S parallel. On the same day, a smaller fragment of the ash cloud appears to be situated north-west of the MBS site, at approximately 60°S, 45°E (Constantine et al. (2000), Fig 8).

It has been established that MBS is climatologically linked to the Southern Indian Ocean (Vance et al., 2016), and atmospheric back trajectory modeling shows that the MBS region regularly receives air masses passing meridionally via the Southern Indian Ocean, and across the Kerguelen Plateau (Jackson et al., 2023). Ten-day HYSPLIT back trajectories computed every 6 hours originating from MBS for 12 - 22 of August, 1991 (dates chosen to coincide with the Cerro Hudson eruption and observed transport of the ash cloud) show multiple trajectories following a path that could reasonably transport Cerro Hudson ash to MBS (Fig. 8). Cluster analysis on 6-hourly trajectories, at 1-hour intervals (resulting in 5 clusters) for the month of August 1991 shows that clusters representing 44% of the trajectories follow a route that would pass through the August 18 Cerro Hudson ash cloud. These transport setups would readily transport very fine grained ash (like the glass shards identified in the MBS-Alpha 1991 sample) towards the MBS site.

HYSPLIT trajectory evidence for long-range atmospheric transport of volcanic ash from the 1991 eruption of Hudson volcano to the MBS site together with our geochemical evidence for similarities between the MBS-Alpha 1991 tephera and Cerro Hudson 1991 tephra provide robust support for our interpretation that the cryptotephra in this layer was produced during the 1991 eruption of Cerro Hudson.

4.3 1985 Horizon

There are no globally significant volcanic eruptions on the order of magnitude of Cerro Hudson or Pinatubo recorded in 1985 to help narrow the search for the source of the glass shards identified in the 1985 horizon. The phonolitic composition of the glass shards is uncommon enough to narrow down the candidates for volcanic source matching. To our knowledge, there are only two phonolitic volcanoes active during the last 1000 years (Global Volcanism Program, 2024). These two volcanoes are the McDonald Islands volcano, located near Heard Island on the Kerguelen Plateau, ∼2000 km NNW of MBS, and Mount Erebus, Ross Island, Antarctica, ∼2500 km SSE of MBS.

There are no known observations of volcanic activity from the McDonald Islands from their discovery in 1874 until 1997. Since 1997, only two eruptive events (Stephenson et al., 2005) have been described, with ongoing hydrothermal activity (Spain et al., 2020). However, the eruptive history of the islands is poorly known due to their extreme remoteness, and near-constant cloud cover in the region making satellite observation difficult for most of the year (Fox et al., 2021).

Mount Erebus has been continuously active since at least 1972 with a maximum VEI of 2, and periods of increased activity from 1984 through 1985 (Global Volcanism Program and McClelland, 1986). Reports from nearby Scott Base describe frequent activity, including the detection of strombolian eruptions, audible explosions, and incandescent ejecta seen from McMurdo Sound and as far away as Butter Point (70 km from the volcano) (Global Volcanism Program and McClelland, 1984).

The phonolite tephra identified in the 1985 horizon show similarities to the composition of volcanic glasses from both Erebus and McDonald Islands (Fig. 9a).

Few analyses of McDonald Islands volcanic material exist in the published literature (Barling et al., 1994; Leach et al., 2016). Leach et al. (2016) investigated an obsidian-rich phonolitic pumice washed up on a beach in the Chatham Islands, Aotearoa, and characterized it as a product of McDonald Islands, likely from the 1997 eruption. Due to the rigorous matching efforts of Leach et al. (2016), and to expand the available match dataset to include recent eruptive products, we include the Chatham Island sample as McDonald for comparison. Analyses from MBS-Alpha 1985 show a less alkaline composition than that of McDonald Islands, largely driven by a lower concentration of Na_2O (Fig. 9). Additionally, MBS-Alpha 1985 has higher concentrations of TiO_2, FeO, and MnO, and generally appears distinct from the literature values for McDonald Islands (Barling et al., 1994; Leach et al., 2016).

The variation diagrams for K_2O, TiO_2, Al_2O_3, Fe_2O_3, MgO, and CaO show that the MBS-Alpha 1985 glass correlates strongly with literature values for Mt. Erebus (Kelly et al., 2008; Harpel et al., 2008; Narcisi et al., 2012; Iverson et al., 2014; Silaev et al., 2020)(Fig. 9). Comparison glass data for Mt. Erebus are sourced from englacial (blue ice and ice core) tephra correlated with Erebus (Harpel et al., 2008; Narcisi et al., 2012; Iverson et al., 2014), lava bombs ejected from 1972-2004 collected near the flanks of Erebus (Kelly et al., 2008), and ash sampled near the crater rim in 2000 (Silaev et al., 2020). While some of the literature shows very stable, homogeneous populations for the products of Mt. Erebus (Iverson et al., 2014), analysis of the 2000 eruption crater rim ash has more highly variable compositions, ranging from phonolitic to trachytic to rhyolitic. Additionally, when whole rock samples are considered (Kyle, 1990; Kyle et al., 1992; Martin et al., 2021), the 1985 tephra fall well within the range of compositions expected from Erebus. MgO bivariate diagrams were also considered

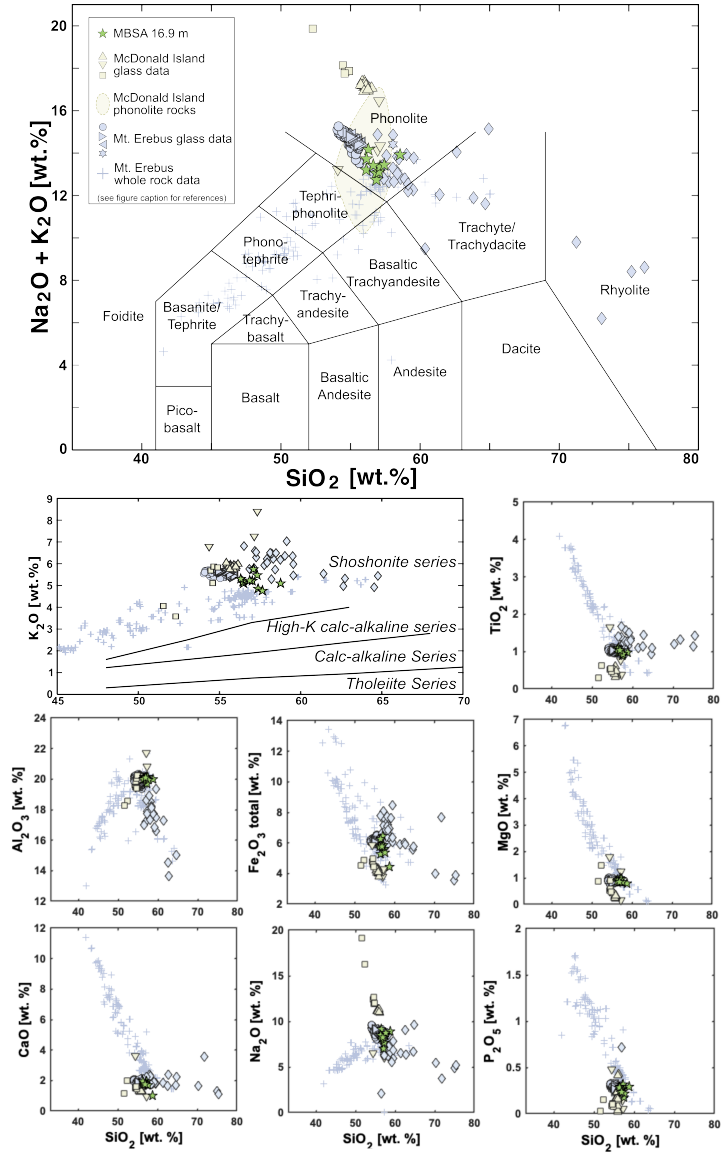

Figure 9. Total alkali-silica diagram (Le Bas et al. (1986)) and individual major element variation diagrams showing the 1985 tephra horizon from MBS-Alpha (green pentagrams, this study), together with literature values for eruptive products from Mt. Erebus (blue right pointing triangles (Kelly et al., 2008), left pointing triangles (Iverson et al., 2014), circles (Harpel et al., 2008), diamonds (Silaev et al., 2020), hexagrams (Narcisi et al., 2012), and pluses (Kyle, 1990; Kyle et al., 1992; Martin et al., 2021)) and McDonald Islands (squares (Leach et al. (2016) McDonald Islands samples), upward pointing triangles (Leach et al. (2016) obsidian floater), and downward pointing triangles (Barling et al., 1994)). Shaded area in TAS diagram shows McDonald Islands phonolite rock compositions (reproduced from Clarke et al. (1983) Figure 3). Discrimination lines on K_2O diagram after Peccerillo and Taylor (1976).

(supplementary materials Figure S.4), and the MBS-Alpha 1985 tephra cluster more strongly with Mt. Erebus products than with those of the McDonald Islands.

4.3.1 1985 Horizon: Atmospheric circulation

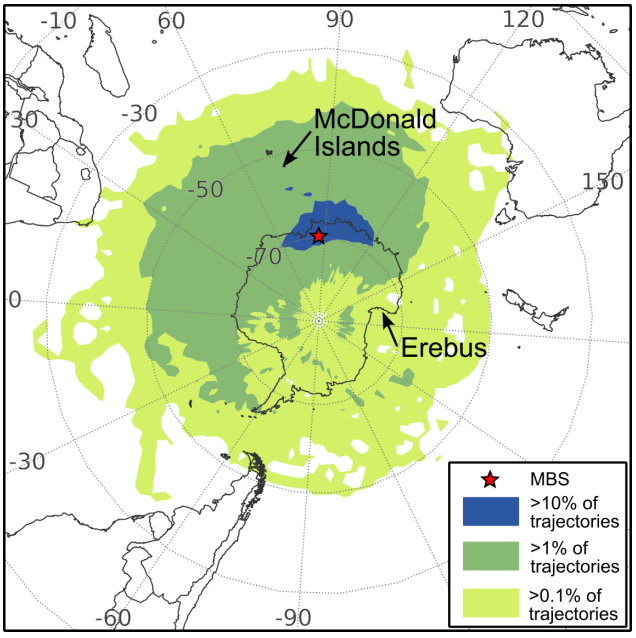

Figure 10. Trajectory frequencies for daily 10-day trajectories from May to December 1985. Frequencies calculated as sum of trajectories passing over a 2-degree gridded area, normalized by the total number of trajectories (856 total trajectories).

Using our general age assessment of mid-late 1985 (Fig. 5) as a starting point, we use HYSPLIT to evaluate potential transport to MBS. Because we do not have an exact eruption date from which to run specific forward trajectories, we use a trajectory frequency analysis here based on a wide date range aimed at encompassing the approximated age of the cryptotephra horizon. Analysis of six-hourly ten day back trajectories for May - December 1985 (856 total trajectories) shows that the MBS site received air masses from a wide range of sources during this period (Fig. 10), including the areas around McDonald Islands and Erebus. Back trajectories from MBS passing over McDonald Islands are more frequent (>1% of trajectories), though some trajectories do pass over Erebus (>0.1%).

Potential transport of any volcanic material produced in the Kerguelen Plateau region is supported by our atmospheric trajectory modeling, showing that a significant proportion of trajectories pass over the Kerguelen Plateau en route to MBS. These trajectories likely represent meridional transport of warm air that frequently bring significant amounts of precipitation to the MBS site (Jackson et al., 2023; Vance et al., 2024a). Transport from Erebus likely follows the polar easterlies commonly seen in the region, which align to the mean wind direction at MBS (Vance et al., 2024a).

Our HYSPLIT trajectory analysis indicates that the MBS-Alpha 1985 tephra could have been transported from a variety of sources, including Mt. Erebus and the McDonald Islands. However, the combination of the major element geochemistry presented here and the known volcanic history of the two potential sources lead to our assessment that the 1985 tephra most likely originated from Mt. Erebus. The potential impact of the identification of Mt. Erebus tephra on our understanding of Antarctic atmospheric transport setups underscores the need for further investigation of the MBS-Alpha 1985 tephra, including trace element analysis.

5 Discussion

5.1 MBS as cryptotephra archive

Here we have identified and described two cryptotephra horizons in the MBS-Alpha ice core which we interpret to be the products of eruptions of Mt. Erebus (1985) and Cerro Hudson (1991). In total, we identified geochemically verifiable tephra in 17% of the samples collected from MBS-Alpha (12 out of 70 samples). Volcanic sulfate and elevated aerosol particle counts have been previously identified in Antarctic ice congruent with the timing of the 1991 eruption of Cerro Hudson (Evangelista et al., 2022; Legrand and Wagenbach, 1999). The MBS 1991 horizon is, to our knowledge, the first geochemically linked identification of Cerro Hudson 1991 glass tephra shards identified in Antarctic ice. Our identification of these cryptotephra horizons highlights both the importance of developing new sampling strategies for locating cryptotephra in ice cores and the potential of the coastal East Antarctic site as a millennial-length archive for future tephrochronology studies.

Tephra and cryptotephra have not been reported for many coastal East Antarctica ice cores. This is because visible tephra layers are uncommon; cryptotephra in these cores tend to be small and sparse, and traditional techniques for identification of cryptotephra require time-consuming, comprehensive sampling of tens to hundreds of meters of ice core material (Cook et al., 2022). Cryptotephra sampling is most often a "needle in a haystack" type of effort, and even in the relatively tephra-rich ice cores from Greenland that are in close proximity to active volcanic centers in Iceland, success rates for tephra sampling efforts are low, especially for broad, comprehensive sampling efforts. It is not uncommon to collect hundreds of samples from a single ice core and identify tephra in as few as 2% of samples (Cook et al., 2022; Coulter et al., 2012). Targeted sampling plans based on ice core chemistry and known eruptions are highly effective in identifying tephra (Abbott et al., 2024), and we demonstrate here that incorporating atmospheric transport into sampling strategies can further improve the likelihood of identifying cryptotephra in ice cores distal to major volcanic sources.

Here, we have incorporated atmospheric modeling tools that enable the hindcasting of atmospheric circulation processes potentially relevant to the cryptotephra transport (over the satellite era). This allowed the development of a sampling strategy tailored to the MBS ice core, by targeting depths where we expected cryptotephra to be found by using the atmospheric transport characteristics of the site to guide sampling together with existing volcanic records and ice core chemistry. The efficiency is gained by the initial atmospheric analysis targeting circulation patterns that would be beneficial to transport to the ice core site as a complementary factor (rather than bulk sampling at low resolution the entire length of the Alpha ice core). Using this initial guidance of episodes of favorable meridional transport from the southern Indian Ocean region to the MBS site, our method

demonstrates the potential of this type of sampling strategy in successfully and more efficiently locating sparse cryptotephra that are not necessarily associated with sulfate or insoluble particle anomalies. We suggest this method could be adapted to other coastal Antarctic ice core locations (such as Roosevelt Island, Fig. 1; Winstrup et al. (2019)) where sampling based on ice core chemistry alone is made challenging by intermittent precipitation or high background levels of marine aerosols.

The presence of volcanic material from Mt. Erebus and Cerro Hudson in the MBS-Alpha ice cores indicates the potential for the preservation of broader Antarctic and ex-Antarctic sources for cryptotephra in East Antarctic ice cores and the MBS ice core array in particular. We expect that other cryptotephra layers exist in the MBS-Alpha ice core, transported by atmospheric pathways not used to guide the sampling performed in this study. Cryptotephra from large, satellite era eruptions outside of our targeted source area (e.g. Puyehue-Cordón Caulle, El Chichón) may exist in MBS-Alpha but were not captured by our method. This is the first tephrochronlogical investigation of MBS ice cores, and provides insight into a region underrepresented in the Antarctic ice core array. Future tephra studies, either from the remaining MBS-Main archive, or from a new core drilled in a similar location, would greatly increase our understanding of the volcanic archive potential of marginal East Antarctic sites. While the available remaining volume of MBS-Main archive is small, (2 cm^2 cross section, a volume often used in tephrochronology studies (Cook et al., 2018)), we propose that our findings here justify using a atmospheric-transport focused sampling to develop a tephrochronology of the deeper section of MBS-Main.

5.2 Tephra transport pathways

Successful preservation of tephra in an ice core relies on an explosive eruption producing an ash plume coinciding with favorable atmospheric circulation patterns to transport the ash to the ice core site. Multiple volcanic factors influence this process including the height of the ash plume, the volume of ash produced, duration of eruption and the location of the volcano relative to the deposition site (Lowe, 2011). In the case of known eruptions, the size of the eruption and the location of the volcano are often the criteria guiding the sampling of Antarctic ice core for tephra and crypotephra, while unknown eruptions are often identified through the presence of associated sulfate and/or insoluble particle anomalies. It has often been expected, however, that only volcanoes erupting in Antarctica or large, globally significant eruptions outside of Antarctica (VEI>5) are likely to be preserved in Antarcic ice cores (Del Carlo et al., 2018). Here we have expanded our sampling strategy to include atmospheric trajectory analysis as a method to successfully sample cryptotephra in ice core. MBS is well suited to test our strategy because we have a strong understanding of the synoptic setups that govern atmospheric transport to the ice core site (Vance et al., 2016; Udy et al., 2021; Jackson et al., 2023).

The atmospheric linkage of coastal East Antarctica and the MBS region with the southern mid-latitudes is well documented (Crockart et al., 2021; Udy et al., 2021; Jackson et al., 2023; Vance et al., 2024a). When the MBS ice core site was selected, one of the selection criteria was the prevalence of teleconnections to lower latitudes, especially capturing interconnectedness with large scale modes of climate variability (including the Southern Annular Mode and the Indian Ocean Dipole; Vance et al. (2016)). The existing body of knowledge about the role of meridional transport (Udy et al., 2021, 2022; Jackson et al., 2023) and the observed coastal easterlies at the MBS site (Vance et al., 2024a) support MBS as a potential cryptotephra archive.

The back trajectory analysis performed in the planning of our study provides evidence that climatological transport pathways linking MBS go beyond its connection with the southern Indian Ocean, and connect the MBS site with a broad range of high latitude air masses. This is consistent with recent investigations that demonstrate that atmospheric rivers and extreme precipitation across the Antarctic continent bring significant heat and precipitation from the sub-tropics and mid-latitudes to polar sites like MBS over short timescales (Wille et al., 2019, 2021; Inda-Díaz et al., 2021; Baiman et al., 2023; Maclennan et al., 2022). The characteristics that made MBS so well suited as a high resolution record of climate variability (Vance et al., 2016; Crockart et al., 2021; Jackson et al., 2023) also increase its chance of preserving tephra from lower latitudes when eruptions coincide with these kinds of atmospheric events.

5.2.1 Meridional transport of Cerro Hudson tephra

The identification of Cerro Hudson tephra in MBS ice verifies the proposed meridional link from MBS to the southern Indian Ocean (Vance et al., 2016). With the Cerro Hudson ash cloud observed over the southern Indian Ocean on August 18, 1991 (Constantine et al., 2000), we interpret that at least some of that ash cloud must have been transported meridionally southwards for deposition at MBS to occur. This meridional transport is validated by HYSPLIT modeling for the period spanning the 1991 horizon, and Neff and Bertler (2015) find that atmospheric transport from Patagonia to the Southern Ocean and Antarctica is highly efficient. This type of meridional transport is especially prevalent during high precipitation days at MBS (Jackson et al., 2023; Vance et al., 2024a). These events are likely to bring any airborne volcanic ash to the ice core site, where it can be deposited by the wet-deposition of tropospheric aerosols characteristic of the MBS site (Crockart et al., 2021).

Cryptotephra from Holocene eruptions of Cerro Hudson have previously been proposed in Antarctic ice cores (Kurbatov et al., 2006; Narcisi et al., 2010, 2012; Evangelista et al., 2022; Abbott et al., 2024). However, some correlations have been refuted, and transport of tephra from low latitudes to Antarctica has been deemed unfeasible based on proposed inability of air masses to penetrate the Antarctic polar jet stream (Del Carlo et al., 2018). Our identification of tephra from the 1991 Cerro Hudson eruption in MBS contradicts this claim, and supports studies on the prevalence of rapid, meridional moisture transport and precipitation to coastal East Antarctica (Wille et al., 2019, 2021; Jackson et al., 2023; Turner et al., 2019). Our results confirming meridional transport support the proposed correlations of other Antarctic ice cores with South American volcanic sources (e.g. Kurbatov et al. (2006); Narcisi et al. (2010, 2012); Evangelista et al. (2022)).

5.2.2 Easterly transport of Mt. Erebus tephra

Transport from Erebus contradicts the general understanding that the majority of atmospheric transport to Antarctica follows the circumpolar westerly winds (Neff and Bertler, 2015). Our finding of tephra transported along this pathway is additionally surprising given the targeting of meridional transport in our sampling strategy, however it is documented that transport to the coastal East Antarctic is complex and often caught up in atmospheric rivers and other cyclonic circulation patterns (Wille et al., 2021; Turner et al., 2019). As evidenced by the HYSPLIT trajectory modeling (Fig. 10), transport from Erebus to MBS occurs relatively infrequently, and primarily in line with the Antarctic polar easterly winds, linked to the southern edge of synoptic scale mid-latitude low pressure systems. These polar easterlies are seen in the mean zonal winds, in line with the snow features

seen and conditions experienced during drilling at the MBS site (Vance et al., 2024a). The identification of MBS-Alpha 1985 tephra as originating from Erebus poses these polar easterly winds as a potentially overlooked mechanism for particle transport to coastal East Antarctic sites.

5.2.3 Further implications

Ice core sites like MBS might preserve tephra from eruptions which (as with Cerro Hudson and Erebus) had been previously thought to be unlikely candidates for the marginal East Antarctic site. Our results demonstrate tephra transport to MBS is viable on the scale of thousands of kilometers by both westerly (from Cerro Hudson) and easterly (from Mt. Erebus) winds. The two cryptotephra horizons identified in the MBS-Alpha core originate from two very distinct source regions. This, combined with the lack of evidence for tephra from other large or more proximal eruptions highlights the importance of favorable atmospheric conditions in the preservation of tephra in ice cores.

While we have identified the 1985 tephra as originating from Erebus, HYSPLIT trajectories from the Heard and McDonald Islands region are more frequent (Fig. 10). The same processes that transported the 1991 tephra from Cerro Hudson could transport ash from McDonald Islands, given an eruption of suitable size. This is seen in the warm air masses regularly transported along this meridional pathway, bringing substantial amounts of snow to the MBS site (Jackson et al., 2023). The lack of identifiably Heard and McDonald Islands tephra in MBS-Alpha indicates that the either recorded satellite-era eruptions of Heard and McDoanld Islands were not substantial enough to be transported, or did not occur when transport conditions were favorable.

5.3 Ice core chronology refinement

The identification of the 1991 Cerro Hudson eruption in the MBS-Alpha ice core has potential implications for ice core dating of both the MBS ice core array and other East Antarctic ice cores. Volcanic events are commonly recognized in ice cores via nssSO_4 (volcanic sulphate) anomalies. Deposition of volcanic sulfate from stratospheric eruptions is relatively spatially homogeneous, and measurable in ice cores using standard ice core chemistry analyses (Lin et al., 2022).These volcanic sulfate records have long been used in the development of robust ice core chronologies, allowing for the synchronization of ice core records across hemispheres (Sigl et al., 2013; Lin et al., 2022).

The use of volcanic sulfate alone in identifying volcanic tie points at annual resolution, however, is not without challenges. Without sulfur isotope analysis, it can be difficult to determine the specific source of nssSO_4 deposition between multiple potential source volcanoes (Lin et al., 2022; Burke et al., 2019). Additionally, volcanic sulfate in ice cores can be altered through diffusion within the ice (Rhodes et al., 2024). Sulfate aerosols from distal sources can take months to years to be deposited, with elevated sulfate levels in ice core chemistry often apparent for multiple years following an eruption (Lin et al., 2022; Svensson et al., 2020; Plunkett et al., 2023; Burke et al., 2019). For example, elevated sulfate concentrations caused by the 1991 eruptions of Cerro Hudson and Pinatubo were found in aerosol measurements at coastal Antarctic stations and in snowfall across the Antarctic Plateau with peaks measured until at least the end of 1993 (Legrand and Wagenbach, 1999). These factors can make defining the precise timing of a volcanic event challenging (Plummer et al., 2012; Sigl et al., 2014, 2015;

Crockart et al., 2021). In the dating of a snowpit record from the Dome Fuji site in East Antarctica Oyabu et al. (2023) were unable to precisely define the Cerro Hudson/Pinatubo volcanic horizon as a dating tie-point due to the presence of three nssSO_4 peaks within a ∼0.5 m interval, likely due to seasonal variability in volcanic sulfate deposition, but possibly also from multiple volcanic eruptions.

Because individual tephra shards can often be geochemically linked to a specific eruption, tephrochronology can help with the refinement of ice core chronologies. Rapid tropospheric transport can carry tephra to an ice core site on the order of days to weeks (Lowe, 2011). If tephra can be identified, it can be used to add precision to sulfate-based chronologies (Geyer et al., 2023; Cook et al., 2022; Lin et al., 2022). Geochemical confirmation of Cerro Hudson as the source of the 1991 horizon confirms the accuracy of the dating of the MBS-Alpha ice core, as the 1991 sample is appropriately linked to mid-1991 in the current MBS chronology (MBS2023, Vance et al. (2024a)). As the time period around 1991 has previously provided challenges with ice core dating (Plummer et al., 2012; Crockart et al., 2021), the ability to assign a specific date to the 1991 cryptotephra horizon identified here could prove instrumental in verifying future ice core dating efforts, and enable the more accurate characterization of climate proxy-signal links in ice core research.

Several globally significant volcanic eruptions have been identified in the sulfate and/or conductivity record of the MBS-Main (Vance et al., 2024a; Harlan et al., 2024a). These eruptions have informed the chronology and synchronization of MBS with other Antarctic ice cores (WAIS, Law Dome, and Roosevelt Island, Vance et al. (2024a)). The identification here of extra-Antarctic (Cerro Hudson) cryptotephra in MBS confirms the potential to locate and identify (crypto)tephra from other globally significant eruptions in the deeper ice of MBS. Identification of any of the volcanic events proposed by Vance et al. (2024a) as volcanic tie-points would have important implications for refinement of the chronology of MBS and other Antarctic ice cores spanning similar time periods.

6 Conclusions

We investigated an East Antarctic ice core for cryptotephra, targeting ice core depths potentially containing cryptotephra using a combination of ice core chemistry, known eruption events, and atmospheric transport modeling. A thorough sampling of the satellite-era Mount Brown South Alpha ice core using this method yielded 42 volcanic glass shards from 12 sample depths. Of these, we present correlations for two samples, each with largely homogeneous compositions. The samples, comprising 10 and 13 glass shards respectively, are proposed to originate from eruptions of Erebus (active throughout the early to mid-1980s) and the 1991 eruption of Cerro Hudson. The identification of two cryptotephra layers in a core spanning only ∼20 m (40 years) is important for future studies due to the relative sparseness of tephra previously identified in East Antarctic ice. This work is a proof of concept for locating and identifying cryptotephra based on this type of targeted sampling, rather than a more time consuming comprehensive screening of an entire ice core.

Identification of tephra at 1985, and its correlation with Mt. Erebus, suggests that the continuing low-level (VEI 1 or 2), Strombolian eruptions occurring at the site have the ability to produce ash that can be transported thousands of kilometers given favorable atmospheric conditions. With appropriate transport conditions, volcanic material can be transported along the

polar easterly winds prevalent at MBS, despite the more frequent events in which warm moist air is advected southwards bringing extreme precipitation to coastal East Antarctica.

Identifying tephra from the 1991 Cerro Hudson eruption in MBS is especially significant for its relevance to ice core dating and core synchronization. The presence of Cerro Hudson tephra shards at 13.28-13.34 m, correlated to 1991, allows definitive confirmation that the MBS-Alpha core is well dated. As this sulfate spike is typically used as a tie point for the early-mid 1990s in Antarctic ice cores, this tephra can confirm or correct the estimate of the important Pinatubo dating horizon. In cases where multiple sulfate peaks are seen around the eruption year, finding Cerro Hudson ash in the core at a depth corresponding to mid-1991 removes any doubt about the timing of sulfate deposition at this site. Additionally, this tephra provides evidence of extra-Antarctic volcanic ash passing the Antarctic circumpolar wind belt to be deposited in Antarctica, previously thought to be improbable.

Our findings position the MBS site (coastal East Antarctica more broadly) as an important potential archive for future tephrochronological work, due to it's high accumulation and teleconnections to such a diverse array of lower latitude source regions. We suggest future targeted sampling of the full MBS-Main core for the development of a comprehensive tephrochronology of coastal East Antarctica. Such a millennial-length tephrocronology would provide a record from a climatologically important region, previously underrepresented in the existing East Antarctic ice core array.

Data availability. The MBS-Alpha Geochemistry datasets produced in this study are available as part of the downloadable supplementary files accompanying this manuscript. The MBS2023 chronology (Vance et al., 2024b) is available at http://dx.doi.org/doi:10.26179/352b-6298. MBS surface core chemistry and water isotope datasets (Moy et al., 2024; Crockart et al., 2021) are available at http://dx.doi.org/doi:10.26179/372t-4q89 and http://dx.doi.org/doi:10.4225/15/58eedf6812621.

Author contributions. MH led the study, including developing the sampling plan and writing the manuscript. MH, TV, JF, and HAK concieved the study. MH and EC prepared ice core samples for analysis at the University of Copenhagen with the help of AS. MH performed sample analysis at the Central Science Laboratory at the University of Tasmania. MH, JF, EC, and AS contributed to geochemical characterization of samples. TV leads the Mount Brown South Ice Core project. All coauthors contributed to writing the manuscript.

Competing interests. The authors declare no competing interests.

Acknowledgements. We thank the members of the Mount Brown South project, including, but not limited to, the team of scientists, technicians, and ice core drillers who made the project possible. Thanks also to Iben Koldtoft for assistance in preparing ice core samples in the freezer laboratory at the University of Copenhagen.

We would also like to acknowledge the contributions of the Central Science Laboratory at the University of Tasmania. The geochemical analysis of the MBS tephra samples in this work would not have been possible without the analytical support of the electron microscopy and x-ray microanalysis group and the expertise of Sandrin Feig. We would also like to thank Sebastien Meffre for sharing expertise on preparation and mounting of fine grained sample material for microanalysis.

This work is supported by the Australian Antarctic Program Partnership funded by the Australian Government as part of the Antarctic Science Collaboration Initiative program (project ID ASCI000002). This project contributes to an Australian Research Council (ARC) Discovery Project (DP220100606). MH is supported by the Australian Antarctic Program Partnership. HAK is supported by the H2020 project TiPES (820970), Horizon Europe project P2F (101184070) and the Danish DFF project (1131-00007B). JF is supported by the Japanese Society for the Promotion of Science through a Postdoctoral Fellowship for Research in Japan.

The Scientific Colour Maps (Crameri, 2023) are used in this study to prevent visual distortion of the data and exclusion of readers with colour-vision deficiencies (Crameri et al., 2020).

References

Abbott, P. M. and Davies, S. M.: Volcanism and the Greenland ice-cores: the tephra record, Earth-Science Reviews, 115, 173–191, https://doi.org/10.1016/j.earscirev.2012.09.001, 2012.

Abbott, P. M., McConnell, J. R., Chellman, N. J., Kipfstuhl, S., Hörhold, M., Freitag, J., Cook, E., Hutchison, W., and Sigl, M.: Mid-to Late Holocene East Antarctic ice-core tephrochronology: Implications for reconstructing volcanic eruptions and assessing their climatic impacts over the last 5,500 years, Quaternary Science Reviews, 329, 108 544, https://doi.org/10.1016/j.quascirev.2024.108544, 2024.

Aoki, K.-I., Yoshida, T., Yusa, K., and Nakamura, Y.: Petrology and geochemistry of the Nyamuragira volcano, Zaire, Journal of Volcanology and Geothermal Research, 25, 1–28, https://doi.org/https://doi.org/10.1016/0377-0273(85)90002-2, 1985.

Baiman, R., Winters, A. C., Lenaerts, J., and Shields, C. A.: Synoptic Drivers of Atmospheric River Induced Precipitation Near Dronning Maud Land, Antarctica, Journal of Geophysical Research: Atmospheres, 128, https://doi.org/10.1029/2022JD037859, 2023.

Barling, J., Goldstein, S. L., and Nicholls, I. A.: Geochemistry of Heard Island (Southern Indian Ocean): Characterization of an Enriched Mantle Component and Implications for Enrichment of the Sub-Indian Ocean Mantle, Journal of Petrology, 35, 1017–1053, https://doi.org/10.1093/petrology/35.4.1017, 1994.

Basile, I., Petit, J. R., Touron, S., Grousset, F. E., and Barkov, N.: Volcanic layers in Antarctic (Vostok) ice cores: Source identification and atmospheric implications, Journal of Geophysical Research: Atmospheres, 106, 31 915–31 931, https://doi.org/10.1029/2000JD000102, 2001.

Burke, A., Moore, K. A., Sigl, M., Nita, D. C., McConnell, J. R., and Adkins, J. F.: Stratospheric eruptions from tropical and extratropical volcanoes constrained using high-resolution sulfur isotopes in ice cores, Earth and Planetary Science Letters, 521, 113–119, https://doi.org/https://doi.org/10.1016/j.epsl.2019.06.006, 2019.

Carn, S. A., Krueger, A. J., Bluth, G. J. S., Schaefer, S. J., Krotkov, N. A., Watson, I. M., and Datta, S.: Volcanic eruption detection by the Total Ozone Mapping Spectrometer (TOMS) instruments: a 22-year record of sulphur dioxide and ash emissions, Geological Society special publication, 213, 177–202, 2003.

Case, P. A., Colarco, P. R., Toon, O. B., and Newman, P. A.: Simulating the Volcanic Sulfate Aerosols From the 1991 Eruption of Cerro Hudson and Their Impact on the 1991 Ozone Hole, Geophysical Research Letters, 51, https://doi.org/10.1029/2023GL106619, 2024.

Castellano, E., Becagli, S., Jouzel, J., Migliori, A., Severi, M., Steffensen, J., Traversi, R., and Udisti, R.: Volcanic eruption frequency over the last 45 ky as recorded in Epica-Dome C ice core (East Antarctica) and its relationship with climatic changes, Global and Planetary Change, 42, 195–205, https://doi.org/https://doi.org/10.1016/j.gloplacha.2003.11.007, ice sheets and neotectonics, 2004.

Clarke, I., McDougall, I., and Whitford, D.: Volcanic evolution of heard and Mc-Donald Islands, Southern Indian Ocean, in: Antarctic earth science. International symposium. 4, pp. 631–635, 1983.

Constantine, E. K., Bluth, G. J. S., and Rose, W. I.: Toms and Avhrr Observations of Drifting Volcanic Clouds from the August 1991 Eruptions of Cerro Hudson, pp. 45–64, American Geophysical Union (AGU), ISBN 9781118664513, https://doi.org/https://doi.org/10.1029/GM116p0045, 2000.

Cook, E., Portnyagin, M., Ponomareva, V., Bazanova, L., Svensson, A., and Garbe-Schönberg, D.: First identification of cryptotephra from the Kamchatka Peninsula in a Greenland ice core: Implications of a widespread marker deposit that links Greenland to the Pacific northwest, Quaternary Science Reviews, 181, 200–206, 2018.

Cook, E., Abbott, P. M., Pearce, N. J., Mojtabavi, S., Svensson, A., Bourne, A. J., Rasmussen, S. O., Seierstad, I. K., Vinther, B. M., Harrison, J., Street, E., Steffensen, J. P., Wilhelms, F., and Davies, S. M.: Volcanism and the Greenland ice cores: A new tephrochronological

framework for the last glacial-interglacial transition (LGIT) based on cryptotephra deposits in three ice cores, Quaternary Science Reviews, 292, 107 596, https://doi.org/10.1016/j.quascirev.2022.107596, 2022.

Coulter, S. E., Pilcher, J. R., Plunkett, G., Baillie, M., Hall, V. A., Steffensen, J. P., Vinther, B. M., Clausen, H. B., and Johnsen, S. J.: Holocene tephras highlight complexity of volcanic signals in Greenland ice cores, Journal of Geophysical Research: Atmospheres, 117, https://doi.org/https://doi.org/10.1029/2012JD017698, 2012.

Crameri, F.: Scientific colour maps, https://doi.org/10.5281/zenodo.8409685, 2023.

Crameri, F., Shephard, G. E., and Heron, P. J.: The misuse of colour in science communication, Nature communications, 11, 5444, 2020.

Crockart, C. K., Vance, T. R., Fraser, A. D., Abram, N. J., Criscitiello, A. S., Curran, M. A. J., Favier, V., Gallant, A. J. E., Kittel, C., Kjær, H. A., Klekociuk, A. R., Jong, L. M., Moy, A. D., Plummer, C. T., Vallelonga, P. T., Wille, J., and Zhang, L.: El Niño–Southern Oscillation signal in a new East Antarctic ice core, Mount Brown South, Climate of the Past, 17, 1795–1818, https://doi.org/10.5194/cp-17-1795-2021, 2021.

Del Carlo, P., Roberto, A. D., D'Orazio, M., Petrelli, M., Angioletti, A., Zanchetta, G., Maggi, V., Daga, R., Nazzari, M., and Rocchi, S.: Late Glacial-Holocene tephra from southern Patagonia and Tierra del Fuego (Argentina, Chile): A complete textural and geochemical fingerprinting for distal correlations in the Southern Hemisphere, Quaternary Science Reviews, 195, 153–170, https://doi.org/10.1016/j.quascirev.2018.07.028, 2018.

Delmonte, B., Baroni, C., Andersson, P., Narcisi, B., Salvatore, M., Petit, J., Scarchilli, C., Frezzotti, M., Albani, S., and Maggi, V.: Modern and Holocene aeolian dust variability from Talos Dome (Northern Victoria Land) to the interior of the Antarctic ice sheet, Quaternary Science Reviews, 64, 76–89, https://doi.org/https://doi.org/10.1016/j.quascirev.2012.11.033, 2013.

Dmitrieva, N., Simonov, V., Safonova, I. Y., Kotlyarov, A., and Karmanov, N.: The Physicochemical Conditions for the Formation of Recent Basalts of Lokon Volcano, Sulawesi Island in the Pacific Ocean: Melt Inclusion Data, Russian Journal of Pacific Geology, 17, 267–283, 2023.

Doiron, S. D., Bluth, G. J. S., Schnetzler, C. C., Krueger, A. J., and Walter, L. S.: Transport of Cerro Hudson SO 2 clouds, Eos, Transactions American Geophysical Union, 72, 489–498, https://doi.org/10.1029/90EO00354, 1991.

Dunbar, N. W., Zielinski, G. A., and Voisins, D. T.: Tephra layers in the Siple Dome and Taylor Dome ice cores, Antarctica: Sources and correlations, Journal of Geophysical Research, 108, https://doi.org/10.1029/2002jb002056, 2003.

Dunbar, N. W., Iverson, N. A., Eaton, A. R. V., Sigl, M., Alloway, B. V., Kurbatov, A. V., Mastin, L. G., McConnell, J. R., and Wilson, C. J. N.: New Zealand supereruption provides time marker for the Last Glacial Maximum in Antarctica, Scientific Reports, 7, 12 238, https://doi.org/10.1038/s41598-017-11758-0, 2017.

Etheridge, D. M., Steele, L. P., Langenfelds, R. L., Francey, R. J., Barnola, J.-M., and Morgan, V. I.: Natural and anthropogenic changes in atmospheric CO2 over the last 1000 years from air in Antarctic ice and firn, Journal of Geophysical Research: Atmospheres, 101, 4115–4128, https://doi.org/https://doi.org/10.1029/95JD03410, 1996.

Evangelista, H., Gastagna, A., Correia, A., Potocki, M., Aquino, F., Alencar, A., Mayewski, P., Kurbatov, A., Jaña, R., Nogueira, J., Licinio, M., Alves, E., and Simões, J. C.: The 1991 explosive Hudson volcanic eruption as a geochronological marker for the Northern Antarctic Peninsula, Anais da Academia Brasileira de Ciências, 94, https://doi.org/10.1590/0001-3765202220210810, 2022.

Fernandez, M. I. and Bitschene, P. R.: Anhidrita, volatiles y composición química de la tefra de la erupción del volcán Hudson (Andes Patagónicos) en agosto de 1991, in: Congreso Geológico Argentino, 12°, Mendoza, Argentina, 10-15 Octubre 1993, pp. 302–306, Asociación Geológica Argentina, 1993.

Fox, J. M., McPhie, J., Carey, R. J., Jourdan, F., and Miggins, D. P.: Construction of an intraplate island volcano: The volcanic history of Heard Island, Bulletin of Volcanology, 83, 37, https://doi.org/10.1007/s00445-021-01452-5, 2021.

Francis, P. W., Wadge, G., and Mouginis-Mark, P. J.: Satellite Monitoring of Volcanoes, pp. 257–298, Springer Berlin Heidelberg, Berlin, Heidelberg, ISBN 978-3-642-80087-0, https://doi.org/10.1007/978-3-642-80087-0_8, 1996.

Gao, C., Robock, A., and Ammann, C.: Volcanic forcing of climate over the past 1500 years: An improved ice core-based index for climate models, Journal of Geophysical Research: Atmospheres, 113, https://doi.org/https://doi.org/10.1029/2008JD010239, 2008.

Gedeon, O., Hulínský, V., and Jurek, K.: Microanalysis of Glass Containing Alkali Ions, Microchimica Acta, 132, 505–510, https://doi.org/10.1007/s006040050050, 2000.

Geyer, A., Di Roberto, A., Smellie, J., Van Wyk de Vries, M., Panter, K., Martin, A., Cooper, J., Young, D., Pompilio, M., Kyle, P., and Blankenship, D.: Volcanism in Antarctica: An assessment of the present state of research and future directions, Journal of Volcanology and Geothermal Research, 444, 107 941, https://doi.org/https://doi.org/10.1016/j.jvolgeores.2023.107941, 2023.

Gkinis, V., Jackson, S., Abram, N. J., Curran, M., Blunier, T., Halan, M., Kjær, H. A., Moy, A., Peensoo, K., Quistgaard, T., Vance, T. R., and Vallelonga, P.: An 1135 year very high-resolution water isotope record of polar precipitation from the Indo-Pacific sector of East Antarctica, Ver. 1,, Australian Antarctic Data Centre, https://doi.org/doi:10.26179/ygeq-1a95, accessed: 2024-09-07, 2024a.

Gkinis, V., Sarah Jackson, N. J. A., Plummer, C., Blunier, T., Harlan, M., Kjær, H. A., Moy, A. D., Peensoo, K. M., Quistgaard, T., Svensson, A., and Vance, T. R.: An East Antarctic, sub-annual resolution water isotope record from the Mount Brown South Ice core, Nature Scientific Data, 11, https://doi.org/doi.org/10.1038/s41597-024-03751-w, 2024b.

Global Volcanism Program: [Database] Volcanoes of the World (v. 5.2.1, (3 July 2024). Distributed by Smithsonian Institution, compiled by Venzke, E., https://doi.org/10.5479/si.GVP.VOTW5-2024.5.2, 2024.

Global Volcanism Program and McClelland, L., eds.: Report on Erebus (Antarctica), vol. 9, Smithsonian Institution, 9 edn., https://doi.org/10.5479/si.GVP.SEAN198409-390020, 1984.

Global Volcanism Program and McClelland, L., eds.: Report on Erebus (Antarctica), vol. 11, Smithsonian Institution, 3 edn., https://doi.org/10.5479/si.GVP.SEAN198603-390020, 1986.

Guo, S., Bluth, G. J. S., Rose, W. I., Watson, I. M., and Prata, A. J.: Re-evaluation of SO 2 release of the 15 June 1991 Pinatubo eruption using ultraviolet and infrared satellite sensors, Geochemistry, Geophysics, Geosystems, 5, https://doi.org/10.1029/2003GC000654, 2004.

Gutiérrez, F., Gioncada, A., Ferran, O. G., Lahsen, A., and Mazzuoli, R.: The Hudson Volcano and surrounding monogenetic centres (Chilean Patagonia): An example of volcanism associated with ridge–trench collision environment, Journal of Volcanology and Geothermal Research, 145, 207–233, https://doi.org/10.1016/j.jvolgeores.2005.01.014, 2005.

Haberle, S. G. and Lumley, S. H.: Age and origin of tephras recorded in postglacial lake sediments to the west of the southern Andes, 44°S to 47°S, Journal of Volcanology and Geothermal Research, 84, 239–256, https://doi.org/10.1016/S0377-0273(98)00037-7, 1998.

Harlan, M., Kjær, H. A., de Campo, A., Svensson, A., Blunier, T., Gkinis, V., Jackson, S., Plummer, C., and Vance, T.: High resolution continuous flow analysis impurity data from the Mount Brown South ice core, East Antarctica, Earth System Science Data Discussions, 2024, 1–20, https://doi.org/10.5194/essd-2024-335, 2024a.

Harlan, M., Kjær, H. A., Vance, T., Gkinis, V., Jackson, S., Blunier, T., Svensson, A., Plummer, C., de Campo, A., and Vallelonga, P.: 1137 years of high-resolution Continuous Flow Analysis impurity data from the Mount Brown South Ice Core, Ver. 1, Australian Antarctic Data Centre, https://doi.org/doi:10.26179/9tke-0s16, accessed: 2024-08-02, 2024b.

Harpel, C., Kyle, P., and Dunbar, N.: Englacial tephrostratigraphy of Erebus volcano, Antarctica, Journal of Volcanology and Geothermal Research, 177, 549–568, https://doi.org/https://doi.org/10.1016/j.jvolgeores.2008.06.001, volcanology of Erebus volcano, Antarctica, 2008.

Humphreys, M. C., Kearns, S. L., and Blundy, J. D.: SIMS investigation of electron-beam damage to hydrous, rhyolitic glasses: Implications for melt inclusion analysis, American Mineralogist, 91, 667–679, https://doi.org/doi:10.2138/am.2006.1936, 2006.

Hutchison, W., Gabriel, I., Plunkett, G., Burke, A., Sugden, P., Innes, H., Davies, S., Moreland, W. M., Krüger, K., Wilson, R., Vinther, B. M., Dahl-Jensen, D., Freitag, J., Oppenheimer, C., Chellman, N. J., Sigl, M., and McConnell, J. R.: High-Resolution Ice-Core Analyses Identify the Eldgjá Eruption and a Cluster of Icelandic and Trans-Continental Tephras Between 936 and 943 CE, Journal of Geophysical Research: Atmospheres, 129, e2023JD040 142, https://doi.org/https://doi.org/10.1029/2023JD040142, e2023JD040142 2023JD040142, 2024.

Inda-Díaz, H. A., O'Brien, T. A., Zhou, Y., and Collins, W. D.: Constraining and Characterizing the Size of Atmospheric Rivers: A Perspective Independent From the Detection Algorithm, Journal of Geophysical Research: Atmospheres, 126, https://doi.org/10.1029/2020JD033746, 2021.

Innes, H. M., Hutchison, W., and Burke, A.: Geochemical analysis of extremely fine-grained cryptotephra: New developments and recommended practices, Quaternary Geochronology, 83, 101 553, https://doi.org/10.1016/j.quageo.2024.101553, 2024.

Iverson, N. A., Kyle, P. R., Dunbar, N. W., McIntosh, W. C., and Pearce, N. J. G.: Eruptive history and magmatic stability of Erebus volcano, Antarctica: Insights from englacial tephra, Geochemistry, Geophysics, Geosystems, 15, 4180–4202, https://doi.org/https://doi.org/10.1002/2014GC005435, 2014.

Iverson, N. A., Kalteyer, D., Dunbar, N. W., Kurbatov, A., and Yates, M.: Advancements and best practices for analysis and correlation of tephra and cryptotephra in ice, Quaternary Geochronology, 40, 45–55, https://doi.org/10.1016/j.quageo.2016.09.008, 2017.

Jackson, S. L., Vance, T. R., Crockart, C., Moy, A., Plummer, C., and Abram, N. J.: Climatology of the Mount Brown South ice core site in East Antarctica: implications for the interpretation of a water isotope record, Climate of the Past, 19, 1653–1675, https://doi.org/10.5194/cp-19-1653-2023, 2023.

Jarosewich, E., Nelen, J., and Norberg, J. A.: Reference Samples for Electron Microprobe Analysis, Geostandards Newsletter, 4, 43–47, https://doi.org/https://doi.org/10.1111/j.1751-908X.1980.tb00273.x, 1980.

Kalnay, E., Kanamitsu, M., Kistler, R., Collins, W., Deaven, D., Gandin, L., Iredell, M., Saha, S., White, G., Woollen, J., Zhu, Y., Leetmaa, A., Reynolds, R., Chelliah, M., Ebisuzaki, W., Higgins, W., Janowiak, J., Mo, K. C., Ropelewski, C., Wang, J., Jenne, R., and Joseph, D.: The NCEP/NCAR 40-Year Reanalysis Project, Bulletin of the American Meteorological Society, 77, 437–471, https://doi.org/10.1175/1520-0477(1996)077<0437:TNYRP>2.0.CO;2, 1996.

Kelly, P. J., Kyle, P. R., Dunbar, N. W., and Sims, K. W.: Geochemistry and mineralogy of the phonolite lava lake, Erebus volcano, Antarctica: 1972–2004 and comparison with older lavas, Journal of Volcanology and Geothermal Research, 177, 589–605, https://doi.org/https://doi.org/10.1016/j.jvolgeores.2007.11.025, volcanology of Erebus volcano, Antarctica, 2008.

Koffman, B. G., Kreutz, K. J., Kurbatov, A. V., and Dunbar, N. W.: Impact of known local and tropical volcanic eruptions of the past millennium on the WAIS Divide microparticle record, Geophys. Res. Lett, 40, 4712–4716, https://doi.org/10.1002/grl.50822, 2013.

Koffman, B. G., Dowd, E. G., Osterberg, E. C., Ferris, D. G., Hartman, L. H., Wheatley, S. D., Kurbatov, A. V., Wong, G. J., Markle, B. R., Dunbar, N. W., Kreutz, K. J., and Yates, M.: Rapid transport of ash and sulfate from the 2011 Puyehue-Cordón Caulle (Chile) eruption to West Antarctica, Journal of Geophysical Research: Atmospheres, 122, 8908–8920, https://doi.org/10.1002/2017JD026893, 2017.

Kratzmann, D. J., Carey, S., Scasso, R., and Naranjo, J.-A.: Compositional variations and magma mixing in the 1991 eruptions of Hudson volcano, Chile, Bulletin of Volcanology, 71, 419–439, https://doi.org/10.1007/s00445-008-0234-x, 2009.

Kratzmann, D. J., Carey, S., Scasso, R. A., and Naranjo, J.-A.: Role of cryptic amphibole crystallization in magma differentiation at Hudson volcano, Southern Volcanic Zone, Chile, Contributions to Mineralogy and Petrology, 159, 237–264, https://doi.org/10.1007/s00410-009-0426-1, 2010a.

Kratzmann, D. J., Carey, S. N., Fero, J., Scasso, R. A., and Naranjo, J.-A.: Simulations of tephra dispersal from the 1991 explosive eruptions of Hudson volcano, Chile, Journal of Volcanology and Geothermal Research, 190, 337–352, https://doi.org/10.1016/j.jvolgeores.2009.11.021, 2010b.

Kuehn, S., Froese, D., and Shane, P.: The INTAV intercomparison of electron-beam microanalysis of glass by tephrochronology laboratories: Results and recommendations, Quaternary International, 246, 19–47, https://doi.org/https://doi.org/10.1016/j.quaint.2011.08.022, enhancing tephrochronology and its application (INTREPID Project): Hiroshi Machida commemorative volume, 2011.

Kurbatov, A. V., Zielinski, G. A., Dunbar, N. W., Mayewski, P. A., Meyerson, E. A., Sneed, S. B., and Taylor, K. C.: A 12,000 year record of explosive volcanism in the Siple Dome Ice Core, West Antarctica, Journal of Geophysical Research: Atmospheres, 111, https://doi.org/https://doi.org/10.1029/2005JD006072, 2006.

Kyle, P.: McMurdo Volcanic Group Western Ross Embayment, chap. A., pp. 18–145, American Geophysical Union (AGU), ISBN 9781118664728, https://doi.org/https://doi.org/10.1029/AR048p0018, 1990.

Kyle, P. R., Moore, J. A., and Thirlwall, M. F.: Petrologic Evolution of Anorthoclase Phonolite Lavas at Mount Erebus, Ross Island, Antarctica, Journal of Petrology, 33, 849–875, https://doi.org/10.1093/petrology/33.4.849, 1992.

Le Bas, M. J., Le Maitre, R. W., Streckeisen, A., Zanettin, B., and IUGS Subcommission on the Systematics of Igneous Rocks: A Chemical Classification of Volcanic Rocks Based on the Total Alkali-Silica Diagram, Journal of Petrology, 27, 745–750, https://doi.org/10.1093/petrology/27.3.745, 1986.

Leach, F., Campbell, H., Eby, N., Holt, K., Regelous, M., Richards, R., and Weaver, S.: Obsidian floater washed up on a beach in the Chatham Islands: geochemical composition and comparison with other volcanic glasses, Tuhinga: Records of the Museum of New Zealand Te Papa Tongarewa, 27, 21–49, 2016.

Lee, G., Burke, A., Hutchison, W., Sugden, P., Smith, C., McConnell, J. R., Sigl, M., Oppenheimer, C., Rasmussen, S. O., Steffensen, J. P., et al.: Phasing and climate forcing potential of the Millennium Eruption of Mt. Baekdu, Communications Earth & Environment, 5, 549, 2024.

Legrand, M. and Wagenbach, D.: Impact of the Cerro Hudson and Pinatubo volcanic eruptions on the Antarctic air and snow chemistry, Journal of Geophysical Research: Atmospheres, 104, 1581–1596, https://doi.org/10.1029/1998JD100032, 1999.

Lin, J., Svensson, A., Hvidberg, C. S., Lohmann, J., Kristiansen, S., Dahl-Jensen, D., Steffensen, J. P., Rasmussen, S. O., Cook, E., Kjær, H. A., Vinther, B. M., Fischer, H., Stocker, T., Sigl, M., Bigler, M., Severi, M., Traversi, R., and Mulvaney, R.: Magnitude, frequency and climate forcing of global volcanism during the last glacial period as seen in Greenland and Antarctic ice cores (60–9 ka), Climate of the Past, 18, 485–506, https://doi.org/10.5194/cp-18-485-2022, 2022.

Lohmann, J. and Svensson, A.: Ice core evidence for major volcanic eruptions at the onset of Dansgaard–Oeschger warming events, Climate of the Past, 18, 2021–2043, https://doi.org/10.5194/cp-18-2021-2022, 2022.

Lowe, D. J.: Tephrochronology and its application: A review, Quaternary Geochronology, 6, 107–153, https://doi.org/10.1016/j.quageo.2010.08.003, 2011.

Luhr, J. F. and Melson, W. G.: Mineral and Glass Compositions in June 15, 1991, Pumices: Evidence for Dynamic Disequilibrium in the Dacite of Mount Pinatubo, in: FIRE and MUD: Eruptions and Lahars of Mount Pinatubo, Philippines, edited by Newhall, C. G. and Punongbayan, R. S., University of Washington Press, 1996.

Maclennan, M. L., Lenaerts, J. T. M., Shields, C., and Wille, J. D.: Contribution of Atmospheric Rivers to Antarctic Precipitation, Geophysical Research Letters, 49, https://doi.org/10.1029/2022GL100585, 2022.

Martin, A. P., Cooper, A. F., Price, R. C., Kyle, P. R., and Gamble, J. A.: Erebus Volcanic Province: petrology, in: Volcanism in Antarctica: 200 Million Years of Subduction, Rifting and Continental Break-up, chap. Chapter 5.2b, Geological Society of London, ISBN 9781786205360, https://doi.org/10.1144/M55-2018-80, 2021.

Matsuoka, K., Skoglund, A., and Roth, G.: Quantarctica [Data set], https://doi.org/10.21334/npolar.2018.8516e961, https://doi.org/10.4225/13/511C71F8612C3, 2018.

McPhie, J., Doyle, M., Allen, R., of Tasmania. Centre for Ore Deposit, U., and Studies, E.: Volcanic Textures: A Guide to the Interpretation of Textures in Volcanic Rocks, Centre for Ore Deposit and Exploration Studies, University of Tasmania, ISBN 9780859015226, https://books.google.ca/books?id=xe9PAQAAIAAJ, 1993.

Moy, A., Vance, T. R., Plummer, C., Jackson, S., Gkinis, V., and Abram, N. J.: The Mount Brown South surface core (MBS1718 'Alpha', 'Bravo', and 'Charlie') chronologies and stable water isotope records, Ver. 1, Australian Antarctic Data Centre, https://doi.org/doi:10.26179/372t-4q89, accessed: 2024-09-07, 2024.

Naranjo S., J. A., Moreno R., H., and Banks, N. G.: La erupción del volcán Hudson en 1991 (46°S) : Región IX, Aisén, Chile, Boletín SERNAGEOMIN, 44, https://bibliotecadigital.ciren.cl/handle/20.500.13082/15896, 1993.

Narcisi, B. and Petit, J. R.: Chapter 6.2: Englacial tephras of East Antarctica, in: Geological Society, London, Memoirs, Volcanism in Antarctica: 200 Million Years of Subduction, Rifting, and Continental Break-up, edited by Smellie, J. L., Panter, K. S., and Geyer, A., vol. 55, pp. 649–664, Geological Society of London, https://doi.org/10.1144/M55-2018-86, 2021.

Narcisi, B., Petit, J., Delmonte, B., Basile-Doelsch, I., and Maggi, V.: Characteristics and sources of tephra layers in the EPICA-Dome C ice record (East Antarctica): Implications for past atmospheric circulation and ice core stratigraphic correlations, Earth and Planetary Science Letters, 239, 253–265, https://doi.org/10.1016/j.epsl.2005.09.005, 2005.

Narcisi, B., Petit, J. R., and Tiepolo, M.: A volcanic marker (92ka) for dating deep east Antarctic ice cores, Quaternary Science Reviews, 25, 2682–2687, https://doi.org/10.1016/j.quascirev.2006.07.009, 2006.

Narcisi, B., Petit, J. R., and Delmonte, B.: Extended East Antarctic ice-core tephrostratigraphy, Quaternary Science Reviews, 29, 21–27, https://doi.org/10.1016/j.quascirev.2009.07.009, 2010.

Narcisi, B., Petit, J. R., Delmonte, B., Scarchilli, C., and Stenni, B.: A 16,000-yr tephra framework for the Antarctic ice sheet: a contribution from the new Talos Dome core, Quaternary Science Reviews, 49, 52–63, https://doi.org/10.1016/j.quascirev.2012.06.011, 2012.

Narcisi, B., Petit, J. R., Delmonte, B., Batanova, V., and Savarino, J.: Multiple sources for tephra from AD 1259 volcanic signal in Antarctic ice cores, Quaternary Science Reviews, 210, 164–174, https://doi.org/https://doi.org/10.1016/j.quascirev.2019.03.005, 2019.

Neff, P. D. and Bertler, N. A. N.: Trajectory modeling of modern dust transport to the Southern Ocean and Antarctica, Journal of Geophysical Research: Atmospheres, 120, 9303–9322, https://doi.org/https://doi.org/10.1002/2015JD023304, 2015.

Oyabu, I., Kawamura, K., Fujita, S., Inoue, R., Motoyama, H., Fukui, K., Hirabayashi, M., Hoshina, Y., Kurita, N., Nakazawa, F., Ohno, H., Sugiura, K., Suzuki, T., Tsutaki, S., Abe-Ouchi, A., Niwano, M., Parrenin, F., Saito, F., and Yoshimori, M.: Temporal variations of surface mass balance over the last 5000 years around Dome Fuji, Dronning Maud Land, East Antarctica, Climate of the Past, 19, 293–321, https://doi.org/10.5194/cp-19-293-2023, 2023.

Paladio-Melosantos, M. L. O., Solidum, R. U., Scott, W. E., Quiambao, R. B., Umbal, J. V., Rodolfo, K. S., Tubianosa, B. S., Reyes, P. J. D., Alonso, R. A., and Ruelo, H. B.: Tephra Falls of the 1991 Eruptions of Mount Pinatubo, in: FIRE and MUD: Eruptions and Lahars of Mount Pinatubo, Philippines, edited by Newhall, C. G. and Punongbayan, R. S., University of Washington Press, 1996.

Palais, J. M., Germani, M. S., and Zielinski, G. A.: Inter-hemispheric Transport of Volcanic Ash from a 1259 A.D. Volcanic Eruption to the Greenland and Antarctic Ice Sheets, Geophysical Research Letters, 19, 801–804, https://doi.org/https://doi.org/10.1029/92GL00240, 1992.

Panaretos, P., Albert, P. G., Thomas, Z. A., Turney, C. S., Stern, C. R., Jones, G., Williams, A. N., Smith, V. C., Hogg, A. G., and Manning, C. J.: Distal ash fall from the mid-Holocene eruption of Mount Hudson (H2) discovered in the Falkland Islands: New possibilities for Southern Hemisphere archive synchronisation, Quaternary Science Reviews, 266, 107 074, https://doi.org/10.1016/j.quascirev.2021.107074, 2021.

Pearce, J. A., Baker, P. E., Harvey, P. K., and Luff, I. W.: Geochemical evidence for subduction fluxes, mantle melting and fractional crystallization beneath the South Sandwich island arc, Journal of Petrology, 36, 1073–1109, 1995.

Peccerillo, A. and Taylor, S. R.: Geochemistry of eocene calc-alkaline volcanic rocks from the Kastamonu area, Northern Turkey, Contributions to Mineralogy and Petrology, 58, 63–81, https://doi.org/10.1007/BF00384745, 1976.

Pitts, M. C. and Thomason, L. W.: The impact of the eruptions of Mount Pinatubo and CERRO Hudson on Antarctic aerosol levels during the 1991 austral spring, Geophysical Research Letters, 20, 2451–2454, https://doi.org/10.1029/93GL02160, 1993.

Piva, S. B., Barker, S. J., Iverson, N. A., Winton, V. H. L., Bertler, N. A., Sigl, M., Wilson, C. J., Dunbar, N. W., Kurbatov, A. V., Carter, L., et al.: Volcanic glass from the 1.8 ka Taupō eruption (New Zealand) detected in Antarctic ice at˜ 230 CE, Scientific Reports, 13, 16 720, 2023.

Plummer, C. T., Curran, M. A. J., van Ommen, T. D., Rasmussen, S. O., Moy, A. D., Vance, T. R., Clausen, H. B., Vinther, B. M., and Mayewski, P. A.: An independently dated 2000-yr volcanic record from Law Dome, East Antarctica, including a new perspective on the dating of the 1450s CE eruption of Kuwae, Vanuatu, Climate of the Past, 8, 1929–1940, https://doi.org/10.5194/cp-8-1929-2012, 2012.

Plunkett, G., Sigl, M., Pilcher, J. R., McConnell, J. R., Chellman, N., Steffensen, J., and Büntgen, U.: Smoking guns and volcanic ash: the importance of sparse tephras in Greenland ice cores, Polar Research, 39, https://doi.org/10.33265/polar.v39.3511, 2020.

Plunkett, G., Sigl, M., McConnell, J. R., Pilcher, J. R., and Chellman, N. J.: The significance of volcanic ash in Greenland ice cores during the Common Era, Quaternary Science Reviews, 301, 107 936, https://doi.org/https://doi.org/10.1016/j.quascirev.2022.107936, 2023.

Poland, M. P., Lopez, T., Wright, R., and Pavolonis, M. J.: Forecasting, detecting, and tracking volcanic eruptions from space, Remote Sensing in Earth Systems Sciences, 3, 55–94, 2020.

Rhodes, R. H., Bollet-Quivogne, Y., Barnes, P., Severi, M., and Wolff, E. W.: New estimates of sulfate diffusion rates in the EPICA Dome C ice core, Climate of the Past, 20, 2031–2043, https://doi.org/10.5194/cp-20-2031-2024, 2024.

Salvioli-Mariani, E., Toscani, L., and Bersani, D.: Magmatic evolution of the Gaussberg lamproite (Antarctica): volatile content and glass composition, Mineralogical Magazine, 68, 83–100, https://doi.org/10.1180/0026461046810173, 2004.

Schoeberl, M. R., Doiron, S. D., Lait, L. R., Newman, P. A., and Krueger, A. J.: A simulation of the Cerro Hudson SO_2 cloud, Journal of Geophysical Research: Atmospheres, 98, 2949–2955, https://doi.org/10.1029/92JD02517, 1993.

Sigl, M., McConnell, J. R., Layman, L., Maselli, O., McGwire, K., Pasteris, D., Dahl-Jensen, D., Steffensen, J. P., Vinther, B., Edwards, R., Mulvaney, R., and Kipfstuhl, S.: A new bipolar ice core record of volcanism from WAIS Divide and NEEM and implications for climate forcing of the last 2000 years, Journal of Geophysical Research: Atmospheres, 118, 1151–1169, https://doi.org/https://doi.org/10.1029/2012JD018603, 2013.

Sigl, M., McConnell, J. R., Toohey, M., Curran, M., Das, S. B., Edwards, R., Isaksson, E., Kawamura, K., Kipfstuhl, S., Krüger, K., et al.: Insights from Antarctica on volcanic forcing during the Common Era, Nature Climate Change, 4, 693–697, 2014.

Sigl, M., Winstrup, M., McConnell, J. R., Welten, K. C., Plunkett, G., Ludlow, F., Büntgen, U., Caffee, M., Chellman, N., Dahl-Jensen, D., et al.: Timing and climate forcing of volcanic eruptions for the past 2,500 years, Nature, 523, 543–549, 2015.

Silaev, V. I., Karpov, G. A., Filippov, V. N., Makeev, B. A., Shanina, S. N., Khazov, A. F., and Tarasov, K. V.: The Mineralogical and Geochemical Properties of Near-Crater Tephra from Erebus Volcano, Antarctica Based on the Ejecta of the 2000 Eruption, Journal of Volcanology and Seismology, 14, 246–261, https://doi.org/10.1134/S0742046320040053, 2020.

Spain, E. A., Johnson, S. C., Hutton, B., Whittaker, J. M., Lucieer, V., Watson, S. J., Fox, J. M., Lupton, J., Arculus, R., Bradney, A., and Coffin, M. F.: Shallow Seafloor Gas emissions Near Heard and McDonald Islands on the Kerguelen Plateau, Southern Indian Ocean, Earth and space science (Hoboken, N.J.), 7, n/a, https://doi.org/10.1029/2019EA000695, 2020.

Stein, A. F., Draxler, R. R., Rolph, G. D., Stunder, B. J. B., Cohen, M. D., and Ngan, F.: NOAA's HYSPLIT Atmospheric Transport and Dispersion Modeling System, Bulletin of the American Meteorological Society, 96, 2059–2077, https://doi.org/10.1175/BAMS-D-14-00110.1, 2015.

Stephenson, J., Budd, G. M., Manning, J., and Hansbro, P.: Major eruption-induced changes to the McDonald Islands, southern Indian Ocean, Antarctic Science, 17, 259–266, https://doi.org/10.1017/S095410200500266X, 2005.

Streeter, R. T., Cutler, N. A., Lawson, I. L., Hutchison, W., Dominguez, L., and Hiles, W.: Glass chemistry of tephra deposits from the 1991 eruption of Hudson, Version 1.0, Interdisciplinary Earth Data Alliance (IEDA), https://doi.org/https://doi.org/10.60520/IEDA/113146, accessed: 2024-19-06, 2024.

Svensson, A., Dahl-Jensen, D., Steffensen, J. P., Blunier, T., Rasmussen, S. O., Vinther, B. M., Vallelonga, P., Capron, E., Gkinis, V., Cook, E., Kjær, H. A., Muscheler, R., Kipfstuhl, S., Wilhelms, F., Stocker, T. F., Fischer, H., Adolphi, F., Erhardt, T., Sigl, M., Landais, A., Parrenin, F., Buizert, C., McConnell, J. R., Severi, M., Mulvaney, R., and Bigler, M.: Bipolar volcanic synchronization of abrupt climate change in Greenland and Antarctic ice cores during the last glacial period, Climate of the Past Discussions, 2020, 1–28, https://doi.org/10.5194/cp-2020-41, 2020.

Tamura, T. and Nakagawa, M.: New petrological and geochemical insights into the magma plumbing system of the 1991 Pinatubo eruption, Contributions to Mineralogy and Petrology, 178, 43, https://doi.org/10.1007/s00410-023-02022-y, 2023.

Turner, J., Phillips, T., Thamban, M., Rahaman, W., Marshall, G. J., Wille, J. D., Favier, V., Winton, V. H. L., Thomas, E., Wang, Z., van den Broeke, M., Hosking, J. S., and Lachlan-Cope, T.: The Dominant Role of Extreme Precipitation Events in Antarctic Snowfall Variability, Geophysical Research Letters, 46, 3502–3511, https://doi.org/https://doi.org/10.1029/2018GL081517, 2019.

Turner, J., Lu, H., King, J. C., Carpentier, S., Lazzara, M., Phillips, T., and Wille, J.: An Extreme High Temperature Event in Coastal East Antarctica Associated With an Atmospheric River and Record Summer Downslope Winds, Geophysical Research Letters, 49, e2021GL097 108, https://doi.org/https://doi.org/10.1029/2021GL097108, e2021GL097108 2021GL097108, 2022.

Udy, D. G., Vance, T. R., Kiem, A. S., Holbrook, N. J., and Curran, M. A. J.: Links between Large-Scale Modes of Climate Variability and Synoptic Weather Patterns in the Southern Indian Ocean, Journal of Climate, 34, 883–889, https://doi.org/10.1175/JCLI-D-20, 2021.

Udy, D. G., Vance, T. R., Kiem, A. S., and Holbrook, N. J.: A synoptic bridge linking sea salt aerosol concentrations in East Antarctic snowfall to Australian rainfall, Communications Earth & Environment, 3, 175, https://doi.org/10.1038/s43247-022-00502-w, 2022.

Udy, D. G., Vance, T. R., Kiem, A. S., Holbrook, N. J., and Abram, N.: Australia's 2019/20 Black Summer fire weather exceptionally rare over the last 2000 years, Communications Earth & Environment, 5, 317, https://doi.org/10.1038/s43247-024-01470-z, 2024.

Vallelonga, P. and Svensson, A.: Ice Core Archives of Mineral Dust, in: Mineral Dust, pp. 463–485, Springer Netherlands, https://doi.org/10.1007/978-94-017-8978-3_18, 2014.

Vance, T. R., Roberts, J. L., Moy, A. D., Curran, M. A., Tozer, C. R., Gallant, A. J., Abram, N. J., Ommen, T. D. V., Young, D. A., Grima, C., Blankenship, D. D., and Siegert, M. J.: Optimal site selection for a high-resolution ice core record in East Antarctica, Climate of the Past, 12, 595–610, https://doi.org/10.5194/cp-12-595-2016, 2016.

Vance, T. R., Abram, N. J., Criscitiello, A. S., Crockart, C. K., DeCampo, A., Favier, V., Gkinis, V., Harlan, M., Jackson, S. L., Kjær, H. A., Long, C. A., Nation, M. K., Plummer, C. T., Segato, D., Spolaor, A., and Vallelonga, P. T.: An annually resolved chronology for the Mount Brown South ice cores, East Antarctica, Climate of the Past, 20, 969–990, https://doi.org/10.5194/cp-20-969-2024, 2024a.

Vance, T. R., Abram, N. J., Gkinis, V., Harlan, M., Jackson, S., Plummer, C., Segato, D., Spolaor, A., Vallelonga, P., Nation, M. K., Long, C., and Kjær, H. A.: MBS2023 - The Mount Brown South ice core chronologies and chemistry data, Ver. 1, Australian Antarctic Data Centre, https://doi.org/doi:10.26179/352b-6298, accessed: 2024-09-07, 2024b.

Warner, M.: Introduction to PySPLIT: A python toolkit for NOAA ARL's HYSPLIT model, Computing in Science & Engineering, 20, 47–62, https://doi.org/10.1109/MCSE.2017.3301549, 2018.

Wille, J. D., Favier, V., Dufour, A., Gorodetskaya, I. V., Turner, J., Agosta, C., and Codron, F.: West Antarctic surface melt triggered by atmospheric rivers, Nature Geoscience, 12, 911–916, https://doi.org/10.1038/s41561-019-0460-1, 2019.

Wille, J. D., Favier, V., Gorodetskaya, I. V., Agosta, C., Kittel, C., Beeman, J. C., Jourdain, N. C., Lenaerts, J. T. M., and Codron, F.: Antarctic Atmospheric River Climatology and Precipitation Impacts, Journal of Geophysical Research: Atmospheres, 126, https://doi.org/10.1029/2020jd033788, 2021.

Wilson, T. M., Cole, J. W., Stewart, C., Cronin, S. J., and Johnston, D. M.: Ash storms: impacts of wind-remobilised volcanic ash on rural communities and agriculture following the 1991 Hudson eruption, southern Patagonia, Chile, Bulletin of Volcanology, 73, 223–239, https://doi.org/10.1007/s00445-010-0396-1, 2011.

Winstrup, M., Vallelonga, P., Kjær, H. A., Fudge, T. J., Lee, J. E., Riis, M. H., Edwards, R., Bertler, N. A. N., Blunier, T., Brook, E. J., Buizert, C., Ciobanu, G., Conway, H., Dahl-Jensen, D., Ellis, A., Emanuelsson, B. D., Hindmarsh, R. C. A., Keller, E. D., Kurbatov, A. V., Mayewski, P. A., Neff, P. D., Pyne, R. L., Simonsen, M. F., Svensson, A., Tuohy, A., Waddington, E. D., and Wheatley, S.: A 2700-year annual timescale and accumulation history for an ice core from Roosevelt Island, West Antarctica, Climate of the Past, 15, 751–779, https://doi.org/10.5194/cp-15-751-2019, 2019.

Zhang, L., Vance, T. R., Fraser, A. D., Jong, L. M., Thompson, S. S., Criscitiello, A. S., and Abram, N. J.: Identifying atmospheric processes favouring the formation of bubble-free layers in the Law Dome ice core, East Antarctica, The Cryosphere, 17, 5155–5173, https://doi.org/10.5194/tc-17-5155-2023, 2023.